Relative Muscle Contributions to Mechanical Work in Ergometer Rowing

Experiment, Modeling, and Analysis

Simon Loose

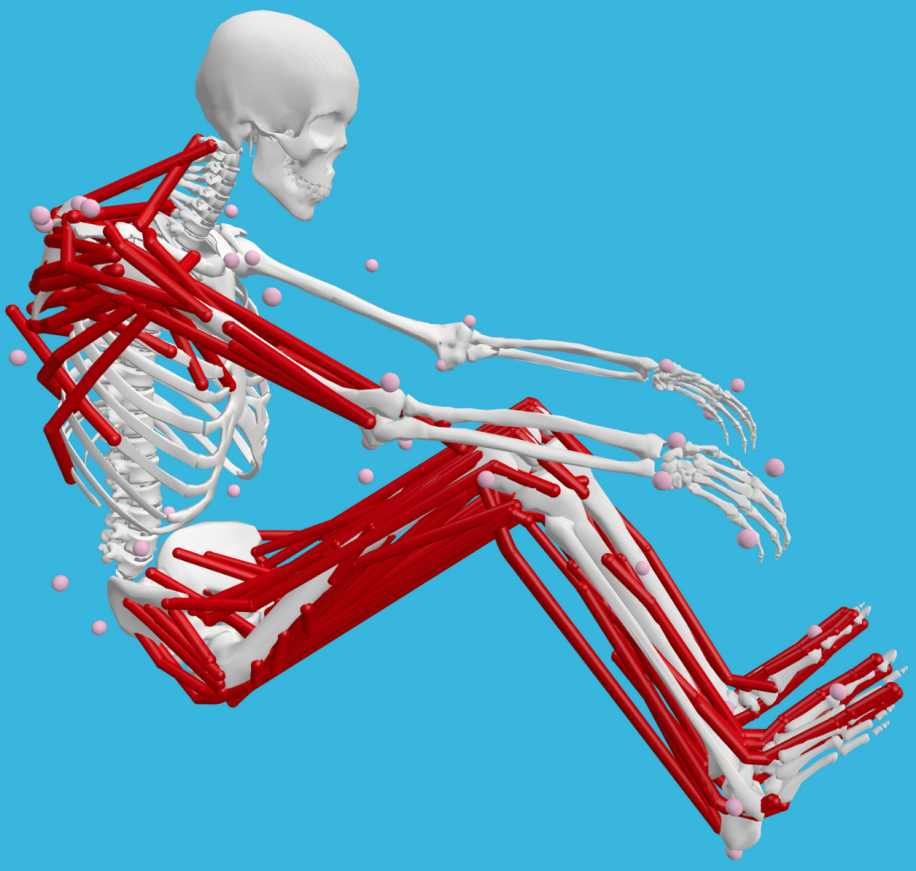

TU Delft

Relative Muscle Contributions to Mechanical Work in Ergometer Rowing

Experiment, Modeling, and Analysis

by

Simon Loose

Supervisors:	Ajay Seth
	Arnoud Greidanus
	Tom Van Wouwe
Project Duration:	December 2023 - August 2025
Faculty:	Faculty of Mechanical Engineering, Delft

TU Delft

Preface

For the past year and a half, I have worked with great excitement on this project. This thesis, just like my master's, took longer than expected due to external circumstances, and also because the project became bigger than we envisioned when we started. Despite the fact that setting up a complete experiment from scratch could be frustrating at times, I am very content that I had the opportunity to be part of the data collection, working directly with our participants. As I hope to continue my career in biomechanics and human movement analysis, it was great to gain experience with measuring a wide variety of biomechanical data.

I wrote this thesis as part of the BioToHydRow project. I would like to thank my supervisors, Arnoud Greidanus and Ajay Seth, for starting this project as a collaboration between the Process & Energy and Biomechanical Engineering departments, as well as for hiring Tom Van Wouwe as a PostDoc on the project to complete the project team. I have greatly enjoyed working with Tom on the experiment, as well as the modeling, and appreciate all his help and the discussions we have had on the project. I also want to thank the project team for being very understanding and supportive when personal struggles popped up, even when they were untimely in the bigger picture of my thesis and our project.

Throughout my thesis, I have always enjoyed discussions with my fellow students from the Computational Biomechanics Lab, as well as with many friends from *De laatste horde* at Dodeka who were also working on their graduation projects. I would particularly like to thank Stefan for motivating each other to get out of the house and study during the summer holiday. I also want to thank Eric and Florian for their feedback towards the end, and working together, albeit on our own projects. Sharing experiences, insights and frustrations made the final weeks far more enjoyable.

Finally, this thesis would not have existed if not for some very important people in my life. I am very thankful to my family for their unconditional support, and for always encouraging a curious and critical attitude, while being open to new ideas and concepts. I specifically want to thank my mother for starting my interest in the human body and its movement, my father for my curiosity into how things work and for reading through my thesis with great attention to detail, and my brother Bernard for our shared passion for sports, which has been strengthened over the years by all the amazing people I have met. Last but not least, I want to thank Jasmijn for being my greatest supporter throughout this project.

Simon Loose
Delft, August 2025

Summary

In running and cycling, efficiency and its dependency upon frequency have been investigated extensively. In rowing however, there is still much to be uncovered. In literature, metabolic efficiency seems to be unaffected by stroke rate, despite theory suggesting the existence of some optimal frequency. In order to better understand the mechanisms behind rowing technique, more research is needed.

Until recently, rowing research was largely conducted through experiments. However, muscle analysis from experimental data alone is limited to EMG data collected during the experiment. With the rise of musculoskeletal models, not only muscle activations, but also other muscle variables can be simulated from kinematics and external forces, enabling muscle analysis in more detail.

This report describes the complete process of gathering comprehensive data in an experiment, processing and preparing this data for use in musculoskeletal simulation, and then using this data to validate the model and generate results. Forces, motion, EMG and breathing gas data are collected with three main goals in mind; to extensively validate the musculoskeletal model, to evaluate muscle contributions to total work across different stroke rates and power outputs, and to assess the effects of stroke rate and power output on muscle contributions and metabolic efficiency.

The experimental results, as well as modeling and simulation outputs, in this report, are in accordance with values reported in literature. Additionally, errors in marker tracking and residual and reserve forces and torques have been found to be within acceptable limits, though it should be noted that errors in the upper body are higher than in the legs. Nevertheless, the model is deemed to be valid for the application of ergometer rowing.

Throughout stroke rates and power outputs, no statistically significant effect of stroke rate or power output on muscle contributions have been found. Additionally, the effects of stroke rate and power output on metabolic efficiency are deemed insignificant. Across all stroke rates and outputs, the quadriceps, and more specifically the Vastus Medialis, have been identified as the largest contributors to total work at the muscle level. At the joint level however, the hips are the main contributors, despite the Vasti only acting at the knee. This illustrates that work is exchanged between joints by tendinous action from biarticular muscles such as the hamstrings, an effect also known as Lombard's paradox.

Contents

Nomenclature

Abbreviations

Abbreviation	Definition
2K	2000 m Ergometer Rowing Time Trial
ANOVA	Analysis of Variance
DOF	Degree Of Freedom
EMG	Electromyography
ID	Inverse Dynamics
IK	Inverse Kinematics
IMU	Inertial Measurement Unit
MAE	Mean Absolute Error
PO	Power Output
PSR	Preferred Stroke Rate
SO	Static Optimization
SR	Stroke Rate

Symbols

Symbol	Definition	Unit
a	Activation level	[-]
C	Coriolis and centrifugal forces	[N]
E	External forces	[N]
e	Efficiency	[-]
e_m	Marker error	[m]
e_q	Coordinate error	[$^\circ$]
F	Force	[N]
f	Maximum force	[N]
G	Gravitational forces	[N]
J	Objective function	[-]
M	Mass	[kg]
MTU	Muscle tendon unit length	[m]
n	Number	[-]
P	Power	[W]
p	Marker position	[m]
q	Coordinate angle	[rad]
$\dot{q}$	Coordinate angular velocity	[rad/s]
$\ddot{q}$	Coordinate angular acceleration	[rad/s^2]
r	Moment arm	[m]
s	Scale factor	[-]
t	Time	[s]
W	Work	[J]
w	Marker error weight	[-]
WPS	Relative work per stroke	[-]
τ	Joint torque	[Nm]
ω	Coordinate error weight	[-]

1

Introduction

Rowing is a popular Olympic endurance sport, with 45.000 members of rowing clubs in the Netherlands alone [38]. Despite its popularity, research into the details of rowing biomechanics at the muscle level is still limited. Understanding these biomechanical principles that drive rowing performance can aid coaches in designing training programs optimized to improve performance while minimizing injury risk.

1.1. Basic biomechanical principles of rowing

In rowing, the goal is to move a boat across a body of water over a certain distance as fast as possible. Blades are moved through the water in a cyclic motion to exert force, propelling the boat forward. This cyclic motion consists of two main phases: a drive phase and a recovery phase [21], [27]. In the drive phase, the blades are submerged, and the rower applies force to the handle. This force is transmitted to the water through the blades, generating a reaction force that causes the boat to accelerate. In the recovery phase, the blades are out of the water, the rower moves his body and the blades back to their initial positions to prepare for the next stroke, and the boat decelerates due to aerodynamic and hydrodynamic drag. From the handle force profile throughout the stroke (Figure 1.1), the drive and recovery phase can be easily distinguished.

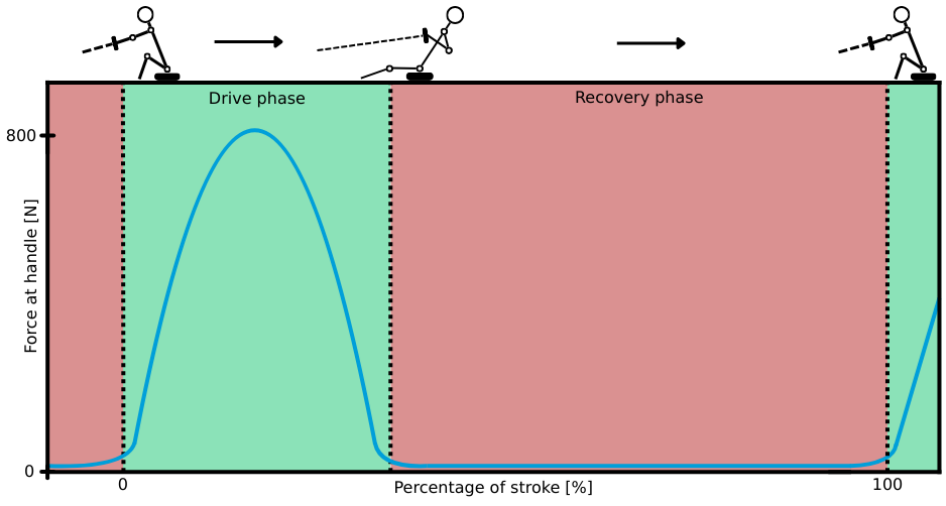

Figure 1.1: Simplified representation of handle force throughout a stroke, clearly showing the distinction between the drive and recovery phase of ergometer rowing. On top of the graph, a sagittal view of the rower is shown at the start of the drive phase, the end of the drive phase, and the end of the recovery phase (i.e. the start of the next drive phase).

Since collecting experimental data during on-water rowing can be challenging due to environmental conditions and physical limitations of measurment equipment, most rowing research is carried out using

ergometers [43]. Rowers often train on rowing ergometers as an alternative to rowing on water [17], despite slight differences in rowing technique between on-water and ergometer rowing [27], [31], [43]. A variety of rowing ergometers are available, with dynamic ergometers gaining popularity in recent years [4], but the use of Concept 2 ergometer is currently the global standard [46].

1.2. Current knowledge on rowing biomechanics

When generating a high power output, optimizing metabolic efficiency enables athletes to maintain high power output for extended periods of time. Since research shows evidence of a metabolically optimal cadence in cycling [3], [5] and metabolically optimal step frequency in running [25], [37], [40], it would be expected that some metabolically optimal stroke rate also exists in rowing. At extremely low stroke rates, the instantaneous power needed to reach some average power output over a stroke would be impossible for a rower to achieve. Given a stroke rate of 1 stroke per minute and a moderate average power output of 250 W, the rower would need to move the handle 10 meters within a single stroke, assuming a constant force of 1500 N, which is higher than the peak force generated during the drive phase by an elite rower [6]. Extremely low stroke rates are thus physically impossible. On the other hand, at extremely high stroke rates, inertia of the upper body would limit the number of strokes per minute. This can be illustrated by an ideal scenario in which muscles can deliver identical and constant force regardless of direction and activate instantly with Figure 1.2a. In this scenario, a small change in lumbar angle of 15° over a stroke is assumed (Figure 1.2b). Assuming an upper body mass of 50 kg with a center of mass at 40 cm above the sacroiliac joint based on Clauser et al. [9] and a joint torque of 400 Nm [12], [19], the amount of strokes would be limited to approximately 85 strokes per minute. This is significantly higher than stroke rates observed in Olympic races, which is around 38 strokes per minute [27]. Theoretically, there must therefore be some optimal frequency somewhere in between these two extremes.

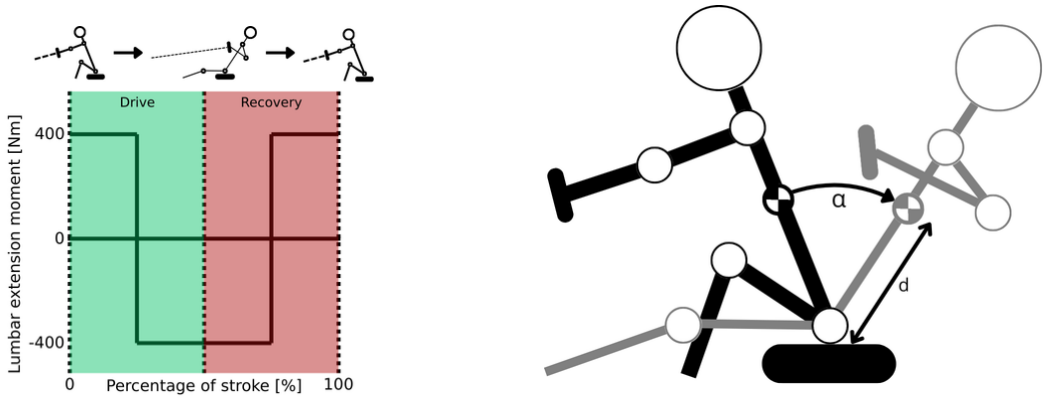

(a) Idealized lumbar moment throughout stroke.

(b) Center of mass distance from sacroiliac joint d and angle α between COM at the start and end of the drive phase.

Figure 1.2: Lumbar moment and geometry illustrating the an ideal scenario, in which forces are constant and instantly applied. Note that his scenario does not take into account forces at the handle.

However, according to Hofmijster et al. [23], there is no significant effect of stroke rate on metabolic efficiency (i.e. mechanical power on the ergometer as a percentage of total metabolic power consumption) during ergometer rowing. This indicates that metabolic efficiency might not be the main driver of preferred or optimal stroke rate. Since rowers clearly show individual preferences in stroke rate, we hypothesize that optimization should occur at the individual muscle level. Identifying muscles that play a key role in rowing performance could be used to identify potential effects of specific muscles' properties (e.g. optimal length or contraction velocity) on stroke rate selection. More insights at the individual muscle level could also be used to find potential areas of improvement in training rowers at any level, especially in terms of increasing performance.

In literature, Quadriceps muscles (specifically Vastus Medialis and Rectus Femoris) have been identified as important drivers of rowing performance [18], [50]. Additionally, Fleming et al. [18] have found that increasing stroke rate leads to increased activations in muscle activity for Rectus Femoris and Vas-

tus Medialis. Similarly, Turpin et al. [48] have found that increasing power output leads to significant increases in muscle activity levels in 22 upper limb, lower limb, and back muscles. However, it should be noted that these experiments control for either stroke rate or power output. Muscle analysis in which stroke rate and power output are controlled simultaneously is yet to be performed.

1.3. Musculoskeletal modeling

Although muscle activations can be measured in experimental setups through electromyography (EMG) [1], [16], [51], the number of muscles that can be analyzed is limited. Additionally, estimating muscle forces is difficult from EMG data alone. Other data often measured in motion analysis research are kinematics, which can be measured directly through motion capture or indirectly through inertial measurement units (IMUs) [29], [45], and forces and moments at the handle, seat and foot stretchers, which can be measured through force sensors or force plates [22], [44]. Using these kinematics and forces, musculoskeletal modeling software can be implemented to calculate muscle activations, forces and more through forward dynamics simulations [2].

OpenSim [15], [42] is an open-source musculoskeletal modeling software package, freely available to anyone. OpenSim uses kinematic and force data to estimate muscle behavior, such as force, length, and activation, that can otherwise be difficult to measure experimentally. A very limited number of OpenSim models used for ergometer rowing exist. Retailleau et al. [39] used an OpenSim model to investigate lower limb kinematics. Although their model does contain leg muscles, the model was not used to estimate muscle forces or activations. The model used by Chandran et al. [7] also focuses on the lower extremity, but aims to estimate tibiofemoral forces during functional electrical stimulation rowing. To achieve this goal, muscle simulations were executed, focused mainly on the hamstrings and quadriceps.

Unfortunately, neither of the OpenSim models mentioned above are freely available. Additionally, to perform extensive analyses on all muscles involved in ergometer rowing, muscles in the upper body should be included as well, as power is transferred from the legs through the upper body and arms to the handle [27]. This calls for the development and validation of a new musculoskeletal ergometer rowing model, in order to investigate muscle contributions throughout the whole body.

1.4. Research goal

This research aims to determine *the relative contributions of muscle work at different stroke rates and power outputs in ergometer rowing*. This goal is attained in three steps. First, an ergometer rowing experiment is specifically designed to collect a comprehensive dataset with experienced rowers. Subsequently, the results from this experiment are used to establish the model's physical validity. Finally, in order to assess these relative contributions, muscle activation and work data obtained from model simulations across stroke rates and power output levels are analyzed.

2

Methods

An ergometer rowing experiment (section 2.1), in which stroke rate (SR) and power output (PO) are controlled, is carried out to collect data. The experimental data is processed and then used to generate and validate results such as muscle activations and forces in an OpenSim model (section 2.2). OpenSim workflow is used to generate these results (section 2.3). Results are then aggregated over trials and participants to compare the conditions controlled in the experiment and identify any significant effects of these conditions on rowing biomechanics (section 2.4). An overview of the data handling process can be found in Figure 2.1.

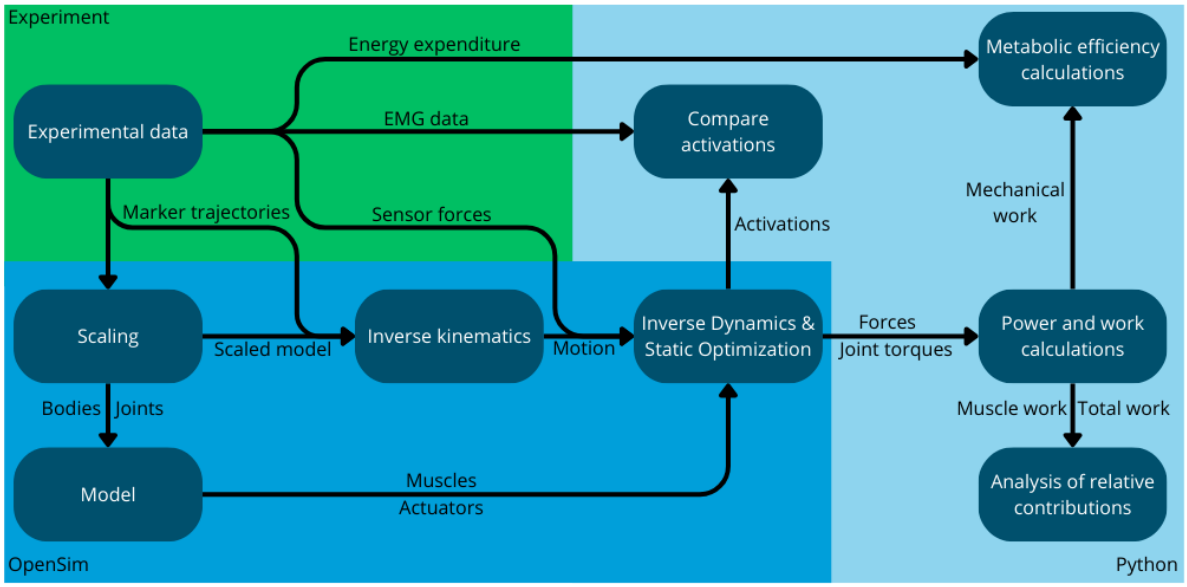

Figure 2.1: Flowchart showing the processing steps from experimental data to results.

2.1. Ergometer rowing experiment

Since existing muskuloskeletal models are based on male individuals [49] and significant differences exist between the male and female musculoskeletal system [35], only male participants were selected to ensure proper representation of participants in model results. Furthermore, all rowers participating in the experiment have at least 2 years of competitive rowing experience.

In running, preferred step frequency is equal to the metabolically optimal step frequency [25], and this also appears to be the case for cycling during prolonged exercise duration [5]. Therefore, in the experiment, rowers will choose their preferred stroke rate (PSR) for a given PO. PO conditions were set

to be low intensity (50% 2K PO) and intermediate training intensity (65% 2K PO), which are both used in daily training. To obtain measurements closer to racing conditions, 75% 2K PO was also examined, though only at PSR.

In the experiment, 14 rowers (all male, 25.31 $\pm$ 3.67 yrs, 189.25 $\pm$ 7.93 cm, 83.94 $\pm$ 7.48 kg, 7.04 $\pm$ 5.64 yrs rowing experience, 370.89 $\pm$ 63.86 W 2K PO) were required to perform 7 rowing trials on a customized Concept2 ergometer at 50%, 65%, and 75% of their average 2K time trial PO. At 50% and 65%, the rowers were tasked with rowing at their PSR, and then at lower (-15% PSR) and higher SR (+15% PSR), while maintaining a steady PO. At 75%, only one trial was performed at PSR. This trial also included 10 strokes in which the rower accelerates towards maximum effort to perform a ”sprint” at the end of the trial. The trials at 50% and 65% are assumed to be at below anaerobic threshold intensity. At 75%, it is likely that the participant will cross this threshold, resulting in substantial anaerobic work, especially during the final 10 strokes of the trial.

As the goal of the experiment was to obtain a comprehensive dataset on ergometer rowing, a measurement setup consisting of four measurement systems was used. Each subsystem is identified in Figure 2.3 and outlined below. Before the start of the experiment, the participant is instrumented with each of these systems.

- *Qualisys motion capture system*
  The motion capture system consists of of 14 cameras in a lab environment and is calibrated at the start of each measurement day. Motion capture data is collected at 100 Hz for a total of 59 markers, of which 43 are on body, 14 on the ergometer to determine the line of action and center of pressure of forces, and 2 on a broomstick used to synchronize motion capture and force data. A full list of markers can be found in Appendix A.
- *Force measurements*
  Three 6DOF AMTI force torque sensors are installed under the seat and foot stretchers (see D in Figure 2.3) to measure forces and moments along all axes at 200 Hz. At the handle, a 1DOF force sensor (see E in Figure 2.3) is mounted to measure pulling force on the chain at 100 Hz.
- *Cometa EMG*
  Muscle excitations are measured for 14 muscles on the right side of the body. Since the rowing motion on the ergometer is essentially symmetric, it is assumed that the muscles on the right side will behave very similarly to their equivalents on the left side. EMG data is collected at 2000 Hz. An overview of the measured muscles is shown in Figure 2.2.
- *Cosmed K5*
  Breathing gases are measured through a breathing mask, which is connected to the Cosmed K5 breathing gas analyzer, worn by the rower on his back. This data can be used to determine metabolic energy consumption during aerobic exercise. The K5 samples at fluctuating frequencies, since it measures in a breath by breath fashion. As metabolic energy consumption can only be inferred from gas analysis while staying below the anaerobic threshold, no breathing gas data is collected during the 75% trial.

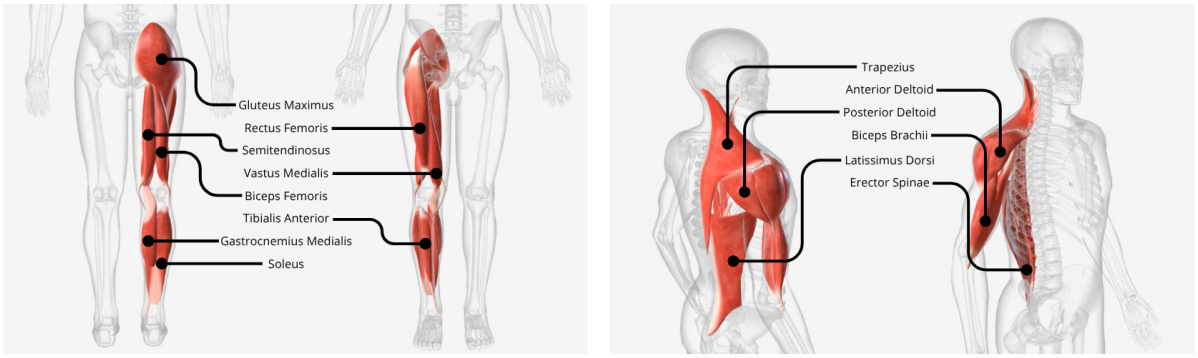

(a) Leg muscles

(b) Shoulder muscles

Figure 2.2: Posterior (left) and anterior (right) view of all muscles measured in the experiment through EMG.

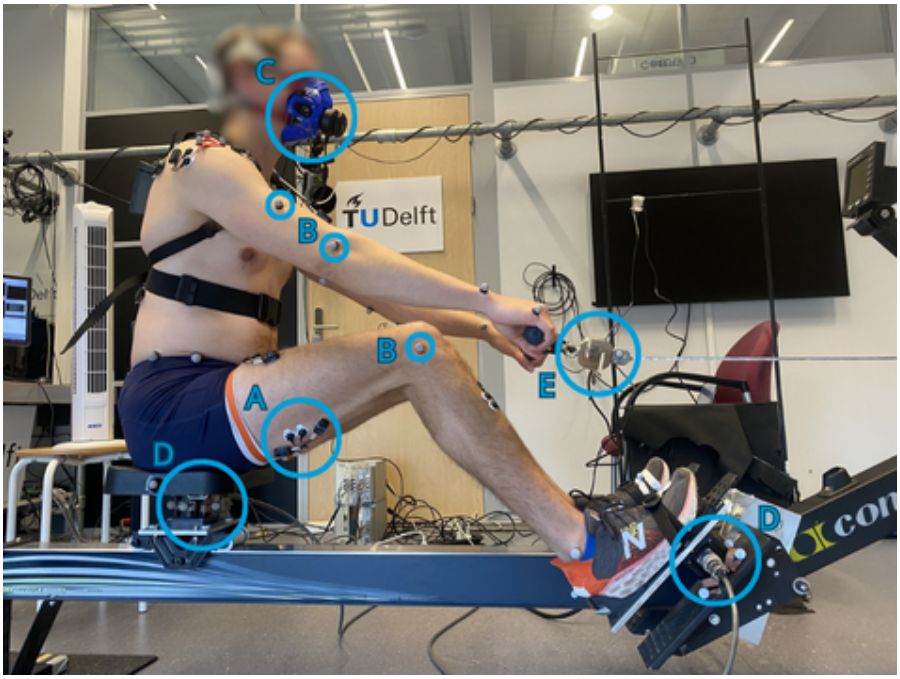

Figure 2.3: Measurement setup, with EMG (A) on muscles on the right side of the body, markers (B), Cosmed breathing mask (C), AMTIs (D) at the feet and seat and handle force sensor (E).

For the analysis in this report, 5 participants were used (27.69 $\pm$ 4.61 yrs, 185.10 $\pm$ 8.75 cm, 82.16 $\pm$ 6.51 kg, 10.90 $\pm$ 7.24 yrs rowing experience, 373.80 $\pm$ 73.43 W 2K PO). In order to analyze all data together in the musculoskeletal model, the data was processed by synchronizing, downsampling, filtering and splitting the data.

Data synchronization

When starting measurements, the motion capture, EMG and handle force data are started simultaneously by a trigger. Since the AMTI force data could not be started at the same time, it is necessary to synchronize the AMTI forces to the rest of the data. This is done by tapping one of the AMTI sensors at the feet using a broomstick with markers on it, inducing peaks in the force measurements, as well as peaks in the acceleration of the markers on the broomstick. These peaks are identified in the data, and forces, motion capture and EMG data are resampled to 100 Hz and cut to the same length, starting from these peaks to the end of the motion capture data, as not all measurements end at the same time. An overview of data synchronization is shown in Figure 2.4.

Since the breathing gases are measured breath by breath, gas data cannot be synchronized to the rest of the data in the same manner. For analysis, only the breaths in the last 100 seconds were used, excluding the final 10 seconds. During these 90 seconds, it is assumed that the rower will have reached a steady state for the targeted SR and PO. Average metabolic power consumption is then calculated over this period.

Data processing

Before experimental data can be used in the model, some data processing steps are required to enable proper analysis of all data types. These data processing steps, all performed in Python, are outlined here.

Measured data inevitably contains noise, which could be amplified when processing data and accelerations in later analysis. Therefore, after synchronization, the forces, motion and EMG data are filtered using a 6 Hz low-pass filter before executing Static Optimization. Additionally, the EMG data is filtered with a 20-400 Hz band-pass filter, as the majority of EMG noise is below 20 Hz and the EMG signal spectrum ranges up to around 400 Hz [13].

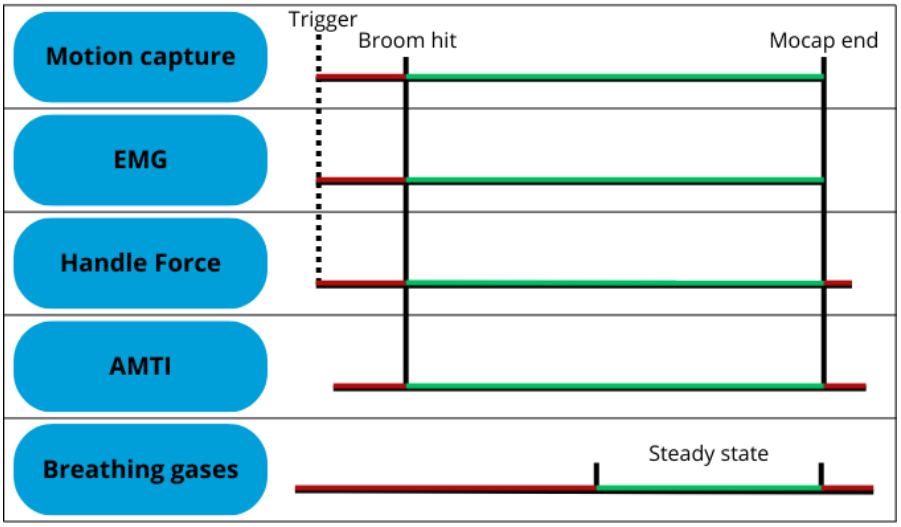

Figure 2.4: Synchronization of different measurement systems. Parts in red are cut from the data, green parts are used for further analysis. *Mocap end* signifies the end of end of motion capture data.

For analysis with the musculoskeletal model, only the middle 10 strokes of the last minute of data for each trial are used. The start of the stroke is considered to be when the handle force starts increasing at the start of the drive phase. The data files are split when force starts increasing at the start of the drive phase and processed per stroke to calculate forces, power and work per muscle, and muscle activations throughout the stroke. After processing, these 10 strokes are aggregated for further analysis. For analysis of muscle and joint actuator work, strokes have also been split into drive and recovery phases. As the drive phase is defined as the period in which work is done by the rower, requiring the rower to exert force on the handle, the transition between drive and recovery is assumed to be when the handle force drops below a threshold of 50 N.

Measurements of energy expenditure can vary by breath, making it impossible to obtain meaningful data on expenditure at specific times during the trial. However, taking the mean of the data over a longer period of time does give a good measure of the average energy expenditure during each trial. As mentioned above, only breaths in the 90 seconds at the end are used for analysis. The average energy expenditure is then calculated over this time period.

As the Cometa EMG measures a voltage, it is necessary to normalize these measurements in order to find an excitation value between 0 and 1. After the filtering described above, EMG data is rectified. Working on the assumption that the measured muscles activate fully during maximal effort ergometer rowing, each signal is normalized by dividing by the maximum value measured for that muscle during the sprint at the end of the 75% trial.

2.2. OpenSim model

The musculoskeletal model used to analyze the data and compute forces, power, and muscle activations is based in OpenSim [15], [42]. The model itself, shown in Figure 2.5, consists of a combination of the RagagopalLaiUhlrich lower body model [49] and the Seth shoulder model [41], with the Brachioradialis muscle added in the shoulder model to make the computation of muscle activations around the elbow joint more realistic. Without Brachioradialis, Biceps Brachii activations would be overestimated, as it is the only other muscle in the model flexing the elbow joint.

The combined model contains 26 bodies, 47 DOFs (including pelvis translations and rotations) and 116 muscle elements. Muscles in both legs and muscles around the right shoulder have been modeled. This combination covers the majority of muscles involved in the rowing motion. The erector spinae muscle is likely the largest contributor to not be included in the model. For the sake of simplicity, the spine of the model is modeled as one rigid element, which likely induces some error in the motion of the torso. In a similar fashion, the wrist joint is not incorporated in the model, causing the forearm and hand

to be modeled as one rigid element without muscles. The Seth shoulder model was applied in order to reduce the error around the shoulders, as rowing involves complex motion of the scapula and clavicle, which a simplified shoulder model would not allow for. A comprehensive overview of the model can be found in Appendix B.

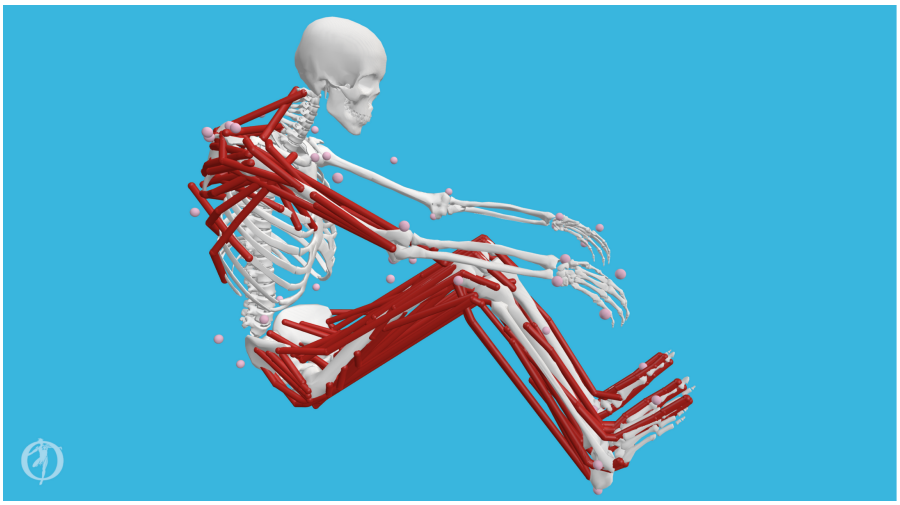

Figure 2.5: OpenSim model showing model geometry, model markers, and all muscle segments in a rowing position.

2.3. Simulation methods

Using the OpenSim model described above, force and marker data from all trials were used to scale the model, track model markers and calculate joint torques, muscle activations and forces. This is done through OpenSims own workflow. Each of these processes is explained below.

Before the model results can be used to analyze muscle dynamics in detail, it is crucial to ensure proper validation for new applications of any model to confirm that model results reflect what is happening in the participant [34]. With this goal in mind, model outputs are validated in several ways throughout the simulation process. Low marker errors from Inverse Kinematics confirm that the kinematics used in further simulation are realistic. Low residuals in Inverse Dynamics and Static Optimization show that external forces are applied correctly, whereas low reserve actuator forces and torques ensure that joints are actuated mainly by muscles, with the reserve actuators playing a supporting role. The final model outputs are validated by correlating muscle activations to experimental EMG measurements.

Scaling

OpenSim's Scaling tool scales body segments in x-, y- and z-direction based on the distances between markers calculated with marker positions from the model's marker set p_m and from experimental marker data p_e. Scale factors are calculated with Equation 2.1. If a segment is scaled based on multiple measurements (e.g. the torso height being scaled with RPSIS-C7 and LPSIS-C7), the total scale factor for this segment will be the average of these measurements (Equation 2.2). All positions related to segments, such as muscle attachment points, are scaled with the same factor as the body segment it is related to. Muscles are then scaled to match the new positions on the scaled bodies. Muscle length properties (i.e. optimal fiber length and tendon slack length) are scaled based on the ratio of the muscle length before and after scaling.

$$s = \frac{|p_{m2} - p_{m1}|}{|p_{e2} - p_{e1}|} \tag{2.1}$$

$$s_{tot} = \frac{\sum_{i=1}^{n} s_i}{n} \tag{2.2}$$

Since mass distribution is preserved, the mass is scaled relative to other body segments, rather than

based on segment scaling. This makes mass scaling a very straightforward process, in which each segment is simply scaled by the ratio of $\frac{m_{new}}{m_{orig}}$, as described in Equation 2.3 below.

$$m_{seg,new} = \frac{m_{new}}{m_{orig}} \cdot m_{seg,orig} \tag{2.3}$$

After scaling, model marker positions are adjusted to match marker positions from experimental data. Through Inverse Kinematics, explained in Equation 2.3, the model is placed in a position matching the experimental data as closely as possible, after which the model markers are moved to the positions of the experimental marker data.

OpenSim's Scaling tool does not scale muscle forces. These are scaled manually through a Python script, changing the maximum force for each muscle in the model based on a muscle scaling law used by Clemente et al. [10]. The scaling factor s_m is calculated using Equation 2.4 and uses the scaled model mass m_{scaled} and the original model mass m_{orig}.

$$s_m = \left(\frac{m_{scaled}}{m_{orig}}\right)^{0.67} \tag{2.4}$$

Inverse Kinematics

The Inverse Kinematics (IK) tool tries to find coordinate values at which the marker errors, as well as the coordinate errors, are minimized by using the weighted least squares equation (Equation 2.7) for each time step. The marker error e_m is defined as the distance between the marker position at the computed coordinate values and experimental marker position (Equation 2.5). The coordinate error e_q is defined as the difference between any tracked coordinate value q_{exp} and its computed coordinate value q (Equation 2.6). Weights are assigned to markers and specific coordinates to specify how strongly a certain marker or coordinate is weighted in minimizing errors.

$$e_m = p_{exp,i} - p_i(q) \tag{2.5}$$

$$e_q = q_{exp,j} - q_j \tag{2.6}$$

$$min \left[\sum_{i=1}^{n_m} w_i \cdot {e_{m,i}}^2 + \sum_{j=1}^{n_q} \omega_j \cdot {e_{q,j}}^2 \right] \tag{2.7}$$

Validation

The output of IK is a set of coordinate values that best match the experimental marker data for each time step. To quantify the quality of this motion, marker errors are analyzed for each marker throughout all measured trials. Hicks et al. [20] suggest that errors should fall within measurement errors, consisting of calibration accuracy [8], skin movement [32] and marker placement errors [14]. With the experimental setup used, error induced by skin movement can amount to several centimeters, especially at the shoulders [36].

Inverse Dynamics

With the model motion from IK and the forces from experimental data, the joint torques needed to have the model perform the motion can be calculated in Inverse Dynamics (ID) from the known masses of model bodies, the motion from IK, and external forces from the experiment. Combining the inertial forces $\mathbf{M\ddot{q}}$, the Coriolis and centrifugal forces $\mathbf{C}$, and the gravitational forces $\mathbf{G}$ with the external forces $\mathbf{E}$ measured at the seat, feet and handle during the experiment gives the equation of motion in Equation 2.8. Measured external forces are applied at the heels for the foot stretchers and at the pelvis for the seat force. Handle force is distributed evenly and applied to the left and right hand.

$$\mathbf{M\ddot{q}} + \mathbf{C}(\mathbf{q}, \dot{\mathbf{q}}) + \mathbf{G}(\mathbf{q}) + \mathbf{E} = \boldsymbol{\tau} \tag{2.8}$$

Validation
In addition to joint torques, ID also outputs residual forces and moments. As the model tracks the motion prescribed by IK, residual actuators at the pelvis are the result of applying Equation 2.8 to pelvis translations and rotations. Residual forces and torques will increase if external forces or model weight are over- or underestimated or if force direction is off. Residual torques will also be elevated by misalignment of the application point of a force or center of mass of model bodies. Low values for residual actuators and the work by residual actuators are thus indicators of properly applied external forces, as well as accurate motion from IK and placement of the center of mass, contributing to higher quality results. This report aims for the work done by residuals to be lower than the 5 largest contributions of muscles used during the drive, to ensure that muscles are the main drivers of work in Static Optimization simulations.

Static Optimization

OpenSim's workflow provides two methods to solve for muscle activations, namely Static Optimization (SO) and Computed Muscle Control (CMC). In essence, CMC is a combination of SO with proportional-derivative control, allowing a more accurate representation of muscles and tendons, as SO assumes tendons to be rigid. As a result, SO requires less computation time, and is generally more user-friendly. SO can thus be seen as a simplified version of CMC. As initial results from SO already showed good agreement with EMG measurements, SO was used to generate compute muscle activations in this research.

In Static Optimization, individual muscle activations a are computed by minimizing the total activation through the objective function in Equation 2.9. Muscles contribute to joint torque by exerting a force $a \cdot f$ (activation times maximum force) at a certain moment arm r_m. Reserve actuators τ_r are added to the model to bridge small gaps between the required joint torques and the contributions of muscles to these torques, and should have small activations, unless a joint is not actuated by muscles. The sum of these muscle contributions, together with the reserve actuators, is equal to the total joint torque τ (Equation 2.10).

$$J = \sum_{m=1}^{n_m} {a_m}^2 \tag{2.9}$$

$$\sum_{m=1}^{n_m} \left[a_m \cdot f\left(F_{m,max}, l_m, v_m\right)\right] r_{m,i} + \tau_{r,i} = \tau_i \tag{2.10}$$

Validation
SO outputs forces and activations for muscles and reserve actuators. In all joints actuated by model muscles, the contributions of reserve actuator torques to total work should be low. Higher torques for reserve actuators might indicate improper muscle scaling, making muscles too weak to fully actuate joints.

The muscle activations from SO can be used to validate muscle activation results throughout the model by computing the correlation and mean absolute error (MAE) with the excitations measured during the experiment with EMG. Since the Erector Spinae muscle is not present in the model, the EMG measurement is compared to the activation of the lumbar extension reserve actuator.

Analyses

From IK and SO, the joint torques, muscle forces and joint angles at every time step are obtained. To perform calculations on power and work from the model, the joint angular velocity and muscle tendon unit length (MTU) are needed as well. These are found by performing a kinematic analysis and a muscle analysis in OpenSim. These analyses essentially evaluate the states of the model and properties of muscles for each timestep during a simulated stroke.

2.4. Simulation output processing

The outputs of the above simulation workflow are forces, activations and kinematics. Some additional processing is necessary to obtain power and work data and assess statistical significance of the simulation results.

2.4.1. Power and work calculations

After performing the analyses, power and work can be calculated for every timestep. For residual and reserve actuators, power P_{act} is calculated by multiplying the joint torque τ by the joint angular velocity $\dot{q}$ (Equation 2.11). Muscle power P_{musc} is calculated by multiplying muscle force F_{musc} by the rate at which MTU shortens for each muscle (contraction velocity, Equation 2.12). To find the total power generated by the model, the power generated by muscles and the power generated by residual and reserve actuators are summed (Equation 2.13). Note that for the power calculated by the model in ID, $\sum_{j=1}^{n_{musc}} P_{musc,j}$ will be zero, whereas for the power generated by the model in SO, the muscle term will be dominant.

$$P_{act} = \tau \cdot \dot{q} \tag{2.11}$$

$$P_{musc} = F_{musc} \cdot -\frac{d(MTU)}{dt} \tag{2.12}$$

$$P_{tot} = \sum_{i=1}^{n_{act}} P_{act,i} + \sum_{j=1}^{n_{musc}} P_{musc,j} \tag{2.13}$$

$$\Delta W_{stroke} = \sum_{i=0}^{n_{timesteps}} P_i \cdot \Delta t \tag{2.14}$$

By integrating power numerically over time throughout the stroke, the work can be found as well. Equation 2.14 was used to calculate the work at the muscle or actuator level. By summing these contributions, work can be calculated at the model level in a similar fashion as Equation 2.13. In the analyses done in this report, W_{stroke} is calculated over the drive phase only (i.e. $n_{timesteps}$ being the number of time steps in the drive phase), as all work contributing to mechanical power at the handle is added during the drive phase.

As another measure of assessing quality of model results, the work done by the residuals relative to the total work done by the model can be compared to the relative contributions from muscles. If residual work is a large portion of the total work done by the model, it is likely to significantly affect the model results, making the computed muscle work unreliable.

Absolute work varies between participants. Therefore, to look into the effects of PO and SR, the work per stroke (WPS) per muscle has been analyzed as a percentage of the total handle work per stroke W_{handle} (Equation 2.15). WPS is grouped by major muscle groups such as quadriceps and hamstrings and muscles with similar functions such as ankle plantarflexors and elbow flexors.

$$WPS_i = \frac{W_{musc,i}}{W_{handle}} \cdot 100\% \tag{2.15}$$

2.4.2. Metabolic efficiency

Since metabolic power consumption was measured during the experiment, the efficiency can be calculated for each trial from the average power delivered at the handle throughout the 10 strokes analyzed for that trial and the average metabolic power consumed during the last 90 seconds of the trial (Equation 2.16). Metabolic efficiency in rowing typically lies between 15% and 20% [22].

$$e_{metabolic} = \frac{P_{handle,avg}}{P_{metabolic}} \cdot 100\% \tag{2.16}$$

2.4.3. Statistical methods

For the analysis of the ID residual forces and torques, WPS values are calculated for all analyzed strokes. Means and standard deviations are then taken over all 10 strokes, all 7 trials and all 5 participants analyzed in this report.

To compare SO activations to EMG measurements, the Pearson correlation coefficient and the mean absolute error (MAE) are calculated for each trial. The mean and standard deviation of the correlation coefficient and MAE are then computed over all strokes, trials and participants. It should be noted that perfect correlation is highly unlikely, due to electromechanical delay [11] between muscle excitation measured by EMG and muscle activation, which is directly linked to force production in SO simulations. Electromechanical delays can reach values around 125 ms, especially when stiffness of muscles and their tendons is taken into account [47].

The effects of SR and PO on the WPS for each muscle group and joint actuator are analyzed by performing a repeated measures analysis of variance (ANOVA) test. The effect on a muscle group or joint is assumed to be significant if $p \leq 0.05$.

3

Results

3.1. Experimental results

Figure 3.1 shows the handle position, force and power of one participant at preferred SR for the three PO conditions and at 65% PO for the three SR conditions throughout the stroke. The handle paths shown in Figure 3.1a and b are comparable to handle paths reported by Cerne et al. [6]. Additionally, the force profiles in Figure 3.1c and d correspond well to the force profile on a Concept2 ergometer from Kleshnev [27].

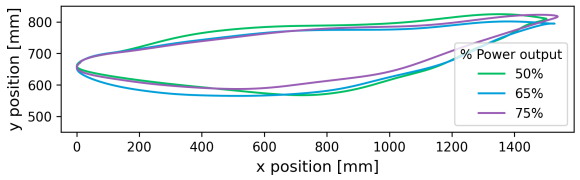

(a) Sagittal view of handle position at preferred SR for different PO conditions.

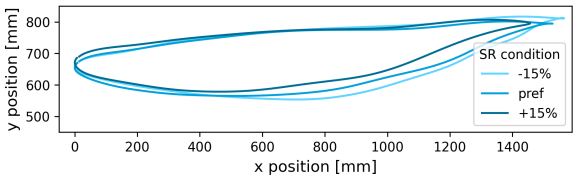

(b) Sagittal view of handle position at 65% PO for different SR conditions.

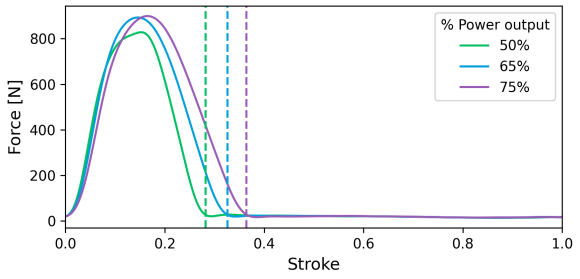

(c) Handle force at preferred SR for different PO conditions.

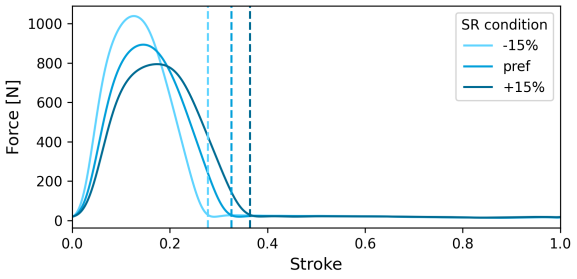

(d) Handle force at 65% PO for different SR conditions.

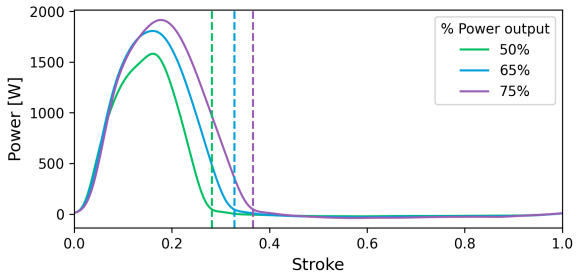

(e) Handle power at preferred SR for different PO conditions.

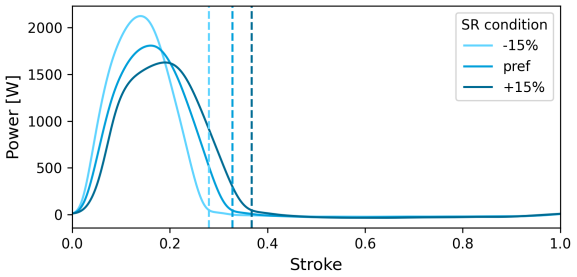

(f) Handle power at 65% PO for different SR conditions.

Figure 3.1: Handle position (a and b), handle force (c and d), and handle power (e and f) throughout the stroke for participant 1. Dashed vertical lines mark the end of the drive phase and the start of the recovery phase.

The force and power profiles show the effect of PO and SR on several important biomechanical variables. First, the peak force and power reached during a stroke increase with PO, as can be seen in Figure 3.1c and e. As average power increases at higher PO and muscles have been reported to activate more at higher PO as well [48], this effect is to be expected. For increasing SR, Figure 3.1d and f show that the peak force and power decrease, as higher SR at constant PO results in lower power per stroke.

PO and SR also affect drive to recovery ratio. The force and power profiles show higher drive to recovery ratios for increasing PO and SR. Hence, in Figure 3.1c, the force does not increase as strongly at higher PO, but the PO is reached by a shorter recovery phase and higher SR. The absolute duration of the drive is not affected by increasing SR. This effect is confirmed by values reported by Cerne et al. on drive to recovery ratio at increasing PO [6].

From these results, it can be observed that to increase PO, rowers increase their peak power as well as their drive to recovery ratio. To increase SR at constant PO, rowers decrease their peak power, but increase drive to recovery ratio to maintain PO.

In Figure 3.2, the metabolic efficiencies of each participant for the different SR and PO conditions are plotted. No universal trend can be observed in Figure 3.2a, which is in accordance with findings by Hofmijster et al. [23]. In Figure 3.2b, there is a significant effect of PO on metabolic efficiency (paired t-test, p=0.011). However, significance is lost when resting metabolic rate is subtracted from average metabolic work (p=0.183).

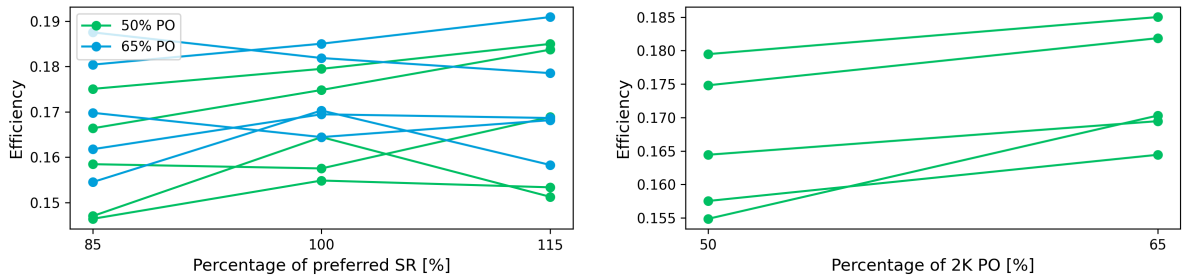

(a) Metabolic efficiency at increasing SR for 50% and 65% PO.

(b) Metabolic efficiency at 50% and 65% PO.

Figure 3.2: Metabolic efficiency at increasing SR (a) and increasing PO (b). Each line represents a participant, with average measurements over trials as dots.

3.2. Validating model results

The first step in validating model results is to investigate marker errors from IK. Figure 3.3 shows the errors for all markers tracked during IK. All median values are below 20 mm, except LClav at 30.6 mm, and C7, RClav, and RHum at 21.3, 21.9, and 22.5 mm respectively. Figure 3.4 shows that for these markers, marker error strongly depends on the phase of the rowing stroke. As the spine is modeled as a rigid body, C7 cannot be properly tracked at the start of the drive phase, when the spine is bent. This also affects adjacent markers, particularly the clavicles. LClav has a higher error than RClav, which is likely due to the higher number of markers on the right shoulder (RClav, ScapTriadL and ScapTriadP), ”pulling” the model slightly to the right to reduce total error.

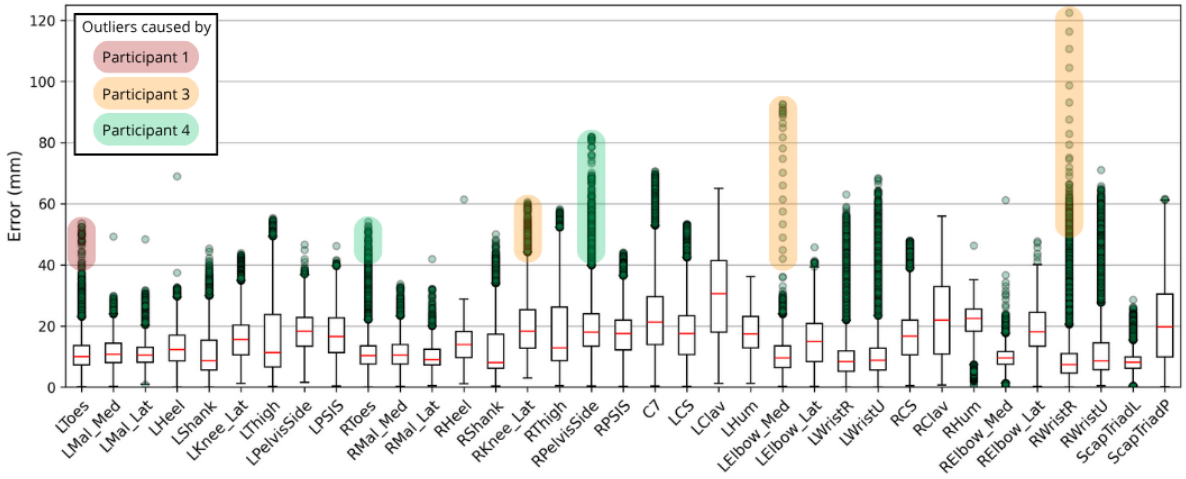

Figure 3.3: Boxplot of IK marker errors for all time points for the 5 participants analyzed in this report. Shaded areas mark ranges of outliers caused by specific participants. For a full list of marker names and locations, see Appendix A.

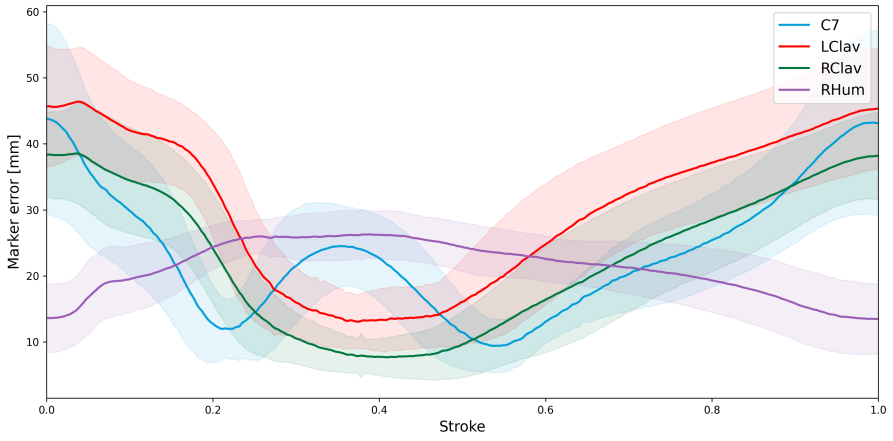

Figure 3.4: Mean marker error over all trials for the 4 markers with highest average error over a stroke. Shaded areas represent one standard deviation above and below the mean.

The highest errors at any time point are mostly accounted for by outliers in specific participants, likely caused by some human error in marker placement. C7 and the wrist markers also show a large amount of outliers. Outliers at the wrist can be explained by the model having no DOF at the wrist, despite some ulnar deviation typically occurring at the end of the drive phase when the handle is pulled close to the chest. Outliers at the shank and thigh are attributed to these markers not placed on bony landmarks. Although such markers move with the skin during measurements, they stay fixed in the model.

After running ID and SO, the first step in validating model outputs is to investigate the residual and reserve actuators. Figure 3.5 shows the aggregated mean and standard deviation of residual work per stroke during the drive phase. As expected, residuals are very low for directions in which little to no movement occurs. Only the work by the force in x-direction and the pelvis tilt moment are elevated, but still below the 5 major muscle contributions to total model work, which implies that the effect of the residuals on simulation results is small.

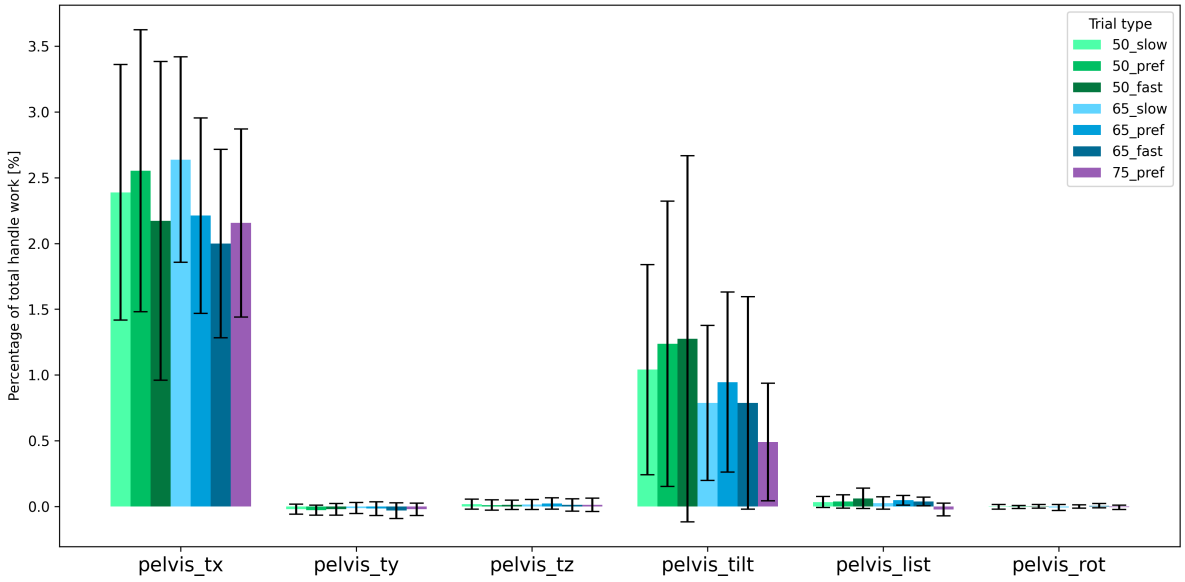

Figure 3.5: Mean and standard deviation of residual WPS averaged over all participants per trial.

The reserve actuators are shown in Figure 3.6. All reserve work at the lower extremity is very low, particularly in comparison to muscle work around the hip and knee joint. In the shoulder, reserves play a more significant role. Since reserve actuators at the elbow are also contributing around 1.5% to the total work, and Brachioradialis is reaching its maximum activation already at 50% PO, it is highly likely that this large contribution is caused by a weak Brachioradialis muscle in the model. Shoulder elevation is also slightly elevated, but below major muscle work contributors around the shoulder.

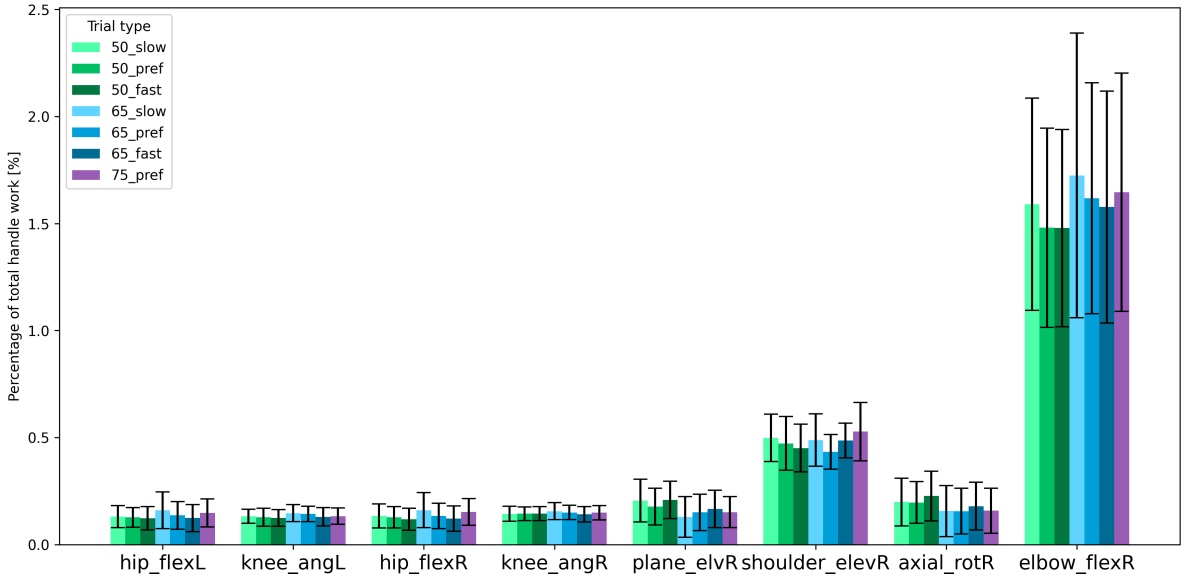

Figure 3.6: Mean and standard deviation of reserve WPS averaged over all participants per trial. Only reserves with a contribution over .2% that are actuated by muscles are included in this figure.

Table 3.1 shows the correlation coefficients and MAE between the muscle activation signal from SO and the excitation signal measured by EMG. The majority of muscles show a clear positive correlation and mean MAE under 0.1, despite offsets between the signals due to electromechanical delay, which are visible in the average activations and excitations over all participants and trials plotted throughout the stroke in Figure 3.7. Especially Soleus, Vastus Medialis, Gluteus Maximus, Posterior Deltoid and

Latissimus Dorsi consistently have high correlation coefficients over all trials and participants. However, the MAE for Gluteus Maximus is much higher, due to a low normalized excitation signal from EMG. This stems from high maximum excitation levels measured during sprint, resulting in low normalized excitation signals.

Table 3.1: Mean and standard deviations of correlation coefficients and mean absolute error (MAE) for all measured muscles between SO results and EMG measurements. Note that the Erector Spinae is correlated to lumbar extension in the model, and thus has no relevant MAE.

	corr	MAE
Tibialis Anterior	0.45 ± 0.34	0.09 ± 0.12
Gastrocnemius Medialis	0.44 ± 0.25	0.08 ± 0.08
Soleus	0.73 ± 0.07	0.09 ± 0.14
Biceps Femoris	0.59 ± 0.14	0.07 ± 0.10
Rectus Femoris	0.16 ± 0.26	0.08 ± 0.09
Vastus Medialis	0.81 ± 0.10	0.06 ± 0.08
Gluteus Maximus	0.72 ± 0.11	0.23 ± 0.27
Semitendinosus	0.31 ± 0.23	0.07 ± 0.10
Erector Spinae*	0.57 ± 0.14	-
Trapezius	0.40 ± 0.20	0.08 ± 0.06
Posterior Deltoid	0.71 ± 0.10	0.05 ± 0.09
Anterior Deltoid	0.29 ± 0.12	0.15 ± 0.16
Biceps Brachii	0.39 ± 0.16	0.06 ± 0.11
Latissimus Dorsi	0.68 ± 0.11	0.05 ± 0.09

Rectus Femoris clearly exhibits lower correlation, and Semitendinosus and Anterior Deltoid have intermediate levels of correlation. Figure 3.7 shows that almost all muscles have a slight delay between the EMG excitation signal and the SO activation signal, which falls within the limits of electromechanical delay as mentioned in subsection 2.4.3. Additionally, potential issues such as measuring adjacent muscles and the model favoring other muscles could contribute to lower correlations.

In addition to the high MAE of Gluteus Maximus, the MAE of Anterior Deltoid is also slightly elevated at 0.15. The EMG excitation signal in Figure 3.7b is consistently higher than the SO activation, because the EMG normalization signal does not actually represent maximum excitation. Anterior Deltoid is primarily activating during the recovery phase. Since all work contributing to powering the ergometer is done during the drive phase and the recovery phase is used to prepare for the next drive by getting back to the first position, the muscles that drive the recovery motion are not activated maximally during the sprint. This increases MAE values, despite low activation values in general.

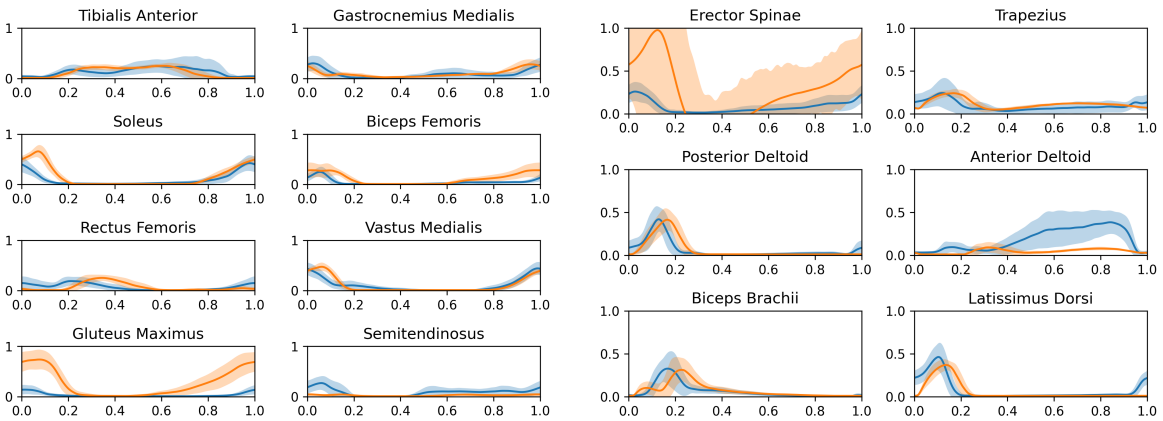

(a) Leg muscles

(b) Shoulder Muscles

Figure 3.7: Average SO activation (orange) and EMG excitation (blue) patterns (y-axis) throughout the stroke (x-axis) over all participants and trials throughout stroke for all measured muscles. Note that the SO activation of Erector Spinae is the signal of the lumbar extension joint actuator, normalized by its maximum value during each stroke.

From Figure 3.7, it is also apparent that all measured muscles, except for Tibialis Anterior, Rectus Femoris, and Anterior Deltoid, activate early on in the stroke, during the drive phase. Rectus Femoris, Tibialis Anterior and Anterior Deltoid activate towards the end of the drive phase and throughout the recovery phase.

From these validation steps, we can conclude the following:

- As marker errors fall within measurement error and larger marker errors are accounted for by model behavior and some marker placement error in specific participants, the motion is deemed to be accurate.
- Evaluation of the contributions of residuals and reserve actuators confirms that their role in the simulations is a supporting one, with the exception of the elbow joint. It can thus be concluded that external forces, as well as the location of the center of mass, have been appropriately applied.
- Correlation and MAE for muscles measured in the experiment and calculated by the model confirm realistic activation patterns and levels from the model, especially considering the offset due to electromechanical delay. If correction for this delay would be taken into account, correlation would likely improve across all muscles.

3.3. Muscle contributions to total work

From the results in Table 3.2, no consistently significant ($p < 0.05$) effects of SR or PO on WPS can be found, both at the joint level and at the muscle level. Elbow flexion at the muscle level is an exception, although it should be noted that this effect is not significant at the joint level.

The work distribution between major muscle groups can be found in Figures 3.8a, 3.9a, and 3.10a. Quadriceps are the largest contributors across all conditions at around 33%, followed by glutes around 15%. Ankle plantarflexors, shoulder muscles, and elbow flexors also contribute up to around 10% of total model work. The reserve actuator of the lumbar joint, where no muscles are modeled, also contribute up to 15% of total work.

The work distribution between joint actuators can be found in Figures 3.8b, 3.9b, and 3.10b. Interestingly, whereas the quadriceps muscles contribute a lot of work at the knee during the drive phase, the hip joint is the greatest contributor to total work at the joint level, adding over 25% of total work. Similarly, the work at the ankle is slightly higher at joint actuator level, whereas the knee joint actuator is relatively low around 10%. This shows a strong dissimilarity to the muscle results, where the quadriceps muscles, acting at the knee, contribute more than thrice this amount.

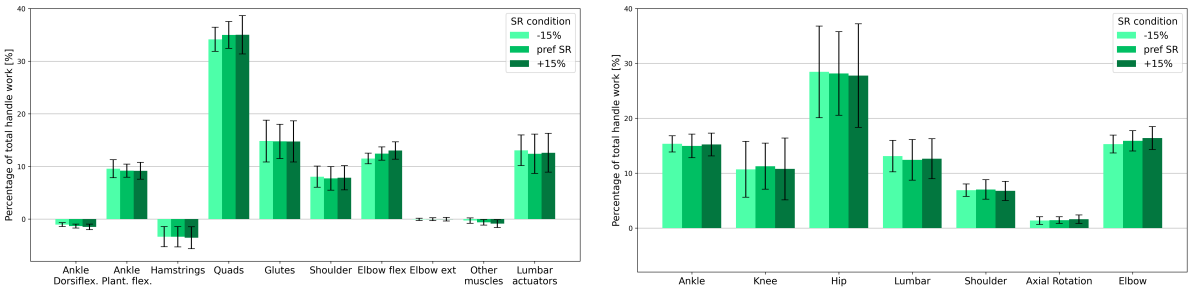

(a) Muscles

(b) ID actuators

Figure 3.8: Mean and standard deviation of WPS for muscle (a) and joint actuator (b) simulation results at 50% PO for different SR conditions.

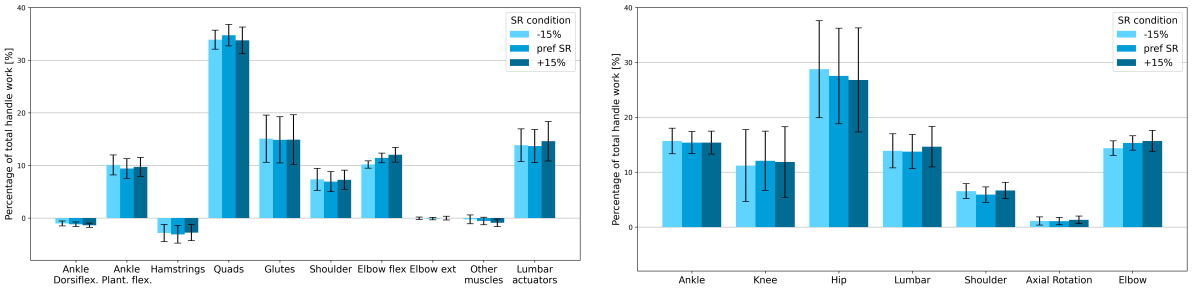

(a) Muscles **(b)** ID actuators

Figure 3.9: Mean and standard deviation of WPS for muscle (a) and joint actuator (b) simulation results at 65% PO for different SR conditions.

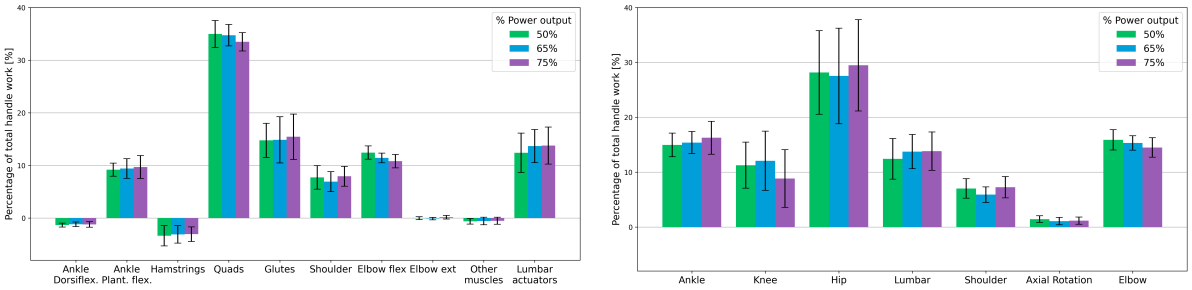

(a) Muscles **(b)** ID actuators

Figure 3.10: Mean and standard deviation of WPS for muscle (a) and joint actuator (b) simulation results at preferred SR for increasing PO.

Table 3.2: Significance levels (p-values) of the effects of SR and PO on muscle WPS (left) and ID actuators WPS (right), as calculated in repeated measures ANOVA testing.

Muscle group	SR at 50%	SR at 65%	PO at preferred SR
Ankle Dorsiflexion	0.5224	0.2816	0.2261
Ankle Plantarflexion	0.4530	0.1602	0.7459
Hamstrings	0.7420	0.0530	0.2600
Quadriceps	0.6868	0.1880	0.3301
Glutes	0.9013	0.6323	0.7057
Shoulder	0.7630	0.1196	0.1369
Elbow Flexion	0.0047	0.0013	0.0119
Elbow Extension	0.3280	0.2052	0.0843

Actuator	SR at 50%	SR at 65%	PO at preferred SR
Ankle	0.7311	0.7599	0.3040
Knee	0.8981	0.7070	0.1964
Hip	0.7556	0.0180	0.6792
Lumbar	0.5388	0.3202	0.0560
Plane Elevation	0.2315	0.4106	0.7883
Shoulder Elevation	0.6322	0.0594	0.1150
Axial Rotation	0.0639	0.1237	0.2053
Elbow	0.1046	0.1144	0.2007

In Figure 3.11, muscles contributing the largest portion of total body work are plotted. It can be seen that Rectus Femoris has a very small contribution compared to the other quadriceps muscles. The quadriceps are driven mostly by Vastus Lateralis, which is also the biggest contributor overall at nearly 25%. Similarly, glutes and ankle plantarflexors are dominated by Gluteus Maximus and Soleus at around 25% and 10% respectively. Shoulder work comes mostly from Teres Major and Posterior Deltoid muscles. Finally, Brachioradialis dominates the elbow flexors, contributing around 10% of total work.

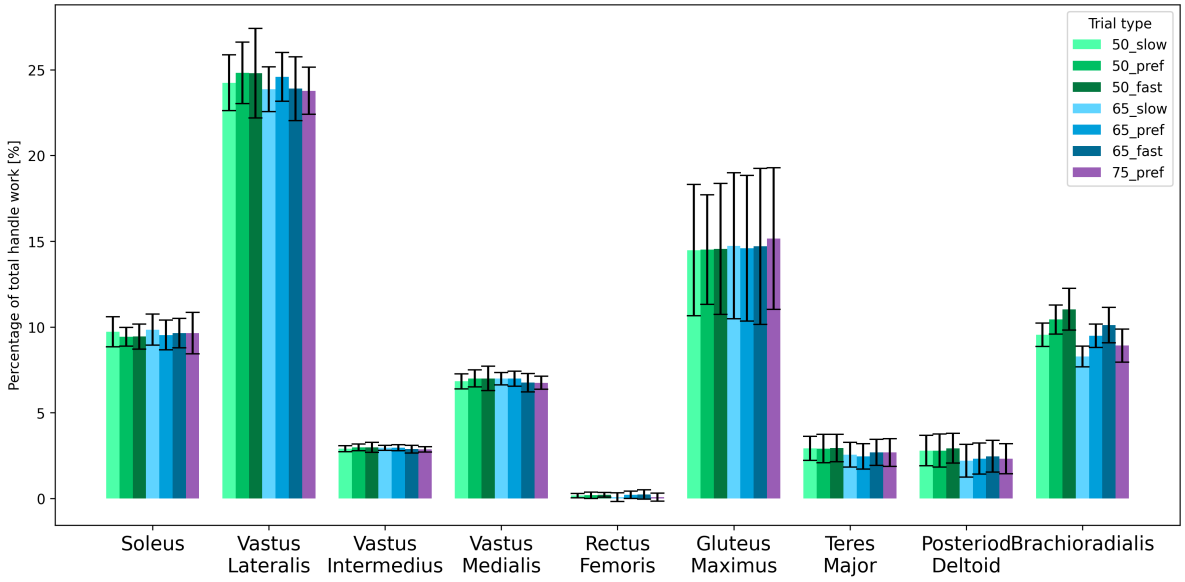

Figure 3.11: Mean and standard deviation of WPS for muscles contributing the most to total model work, including all quadriceps muscles and all contributions over 1%.

4

Discussion

4.1. Relative muscle contributions

The aim of this report was to determine relative muscle contributions of muscle work at different stroke rates and power outputs in ergometer rowing. From the results in Figures 3.8-3.10, the quadriceps can clearly be identified as the largest contributor to total work, providing around 33% of the total work, more than double the amount of other individual muscle groups. The glutes are also strong contributors around 15%, with ankle plantarflexors, elbow flexors, and shoulder muscles contributing slightly less. The contribution of the lumbar actuators suggests that lower back muscles also deliver an important contribution to total muscle work during ergometer rowing.

At the muscle level in Figure 3.11, Vastus Lateralis stands out as the main contributor to total muscle work. Gluteus Maximus plays a big role at the hip joint, and Soleus is the main calf muscle involved in generating power during ergometer rowing. Brachioradialis contributes a large amount of work at the elbow, despite it reaching maximum activation at low intensity. If Brachioradialis were to have an appropriate maximum force, its contribution would likely be increased by 1.5-2%, which is the current contribution of the elbow flexion reserve actuator.

Looking at the other quadriceps muscles, we see that Vastus Intermedius and Vastus Medialis add about 10% of total model work, whereas Rectus Femoris does not contribute any work during the drive. This shows a clear distinction between the Vasti as monoarticular muscles and Rectus Femoris as a biarticular muscle, involved in extending the knee and flexing the hip joint (Figure 4.1a). Since Rectus Femoris activates primarily in the late drive phase, as can be seen in Figure 3.7a, it is likely that its main function during a rowing cycle is to decelerate hip extension at the end of the drive, with other muscles activating to flex the knee.

The hamstrings, as biarticular antagonists of the quadriceps, induce both knee flexion and hip extension. In Figures 3.8a, 3.9a, and 3.10a, the hamstrings can be seen to perform negative work during the drive phase. This might seem counterintuitive, as the hamstrings are working against the production of knee extension moment by the quadriceps, but this can be explained by considering the hamstring as tendons (i.e. passive, strap-like elements). This supports the theory described as Lombard's paradox [30], [33], stating that biarticular muscles act as tendons, allowing monoarticular muscles to also actuate other joints. Figure 4.1 illustrates this effect, showing the Vasti, Rectus Femoris, and hamstring muscles. In this example, shown in Figure 4.1b, tendinous action from the hamstrings enables the Vasti to induce simultaneous hip and knee extension, as the hamstrings do negative work as they extend the hip while being stretched due to knee extension.

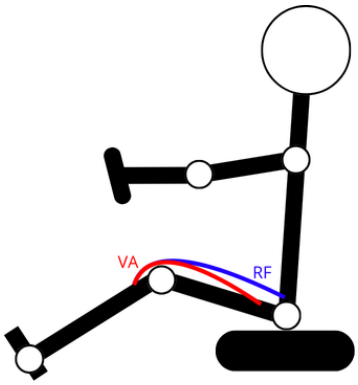

(a) Difference in attachment points of the quadriceps, showing the monoarticular Vasti (VA) and the biarticular Rectus Femoris (RF).

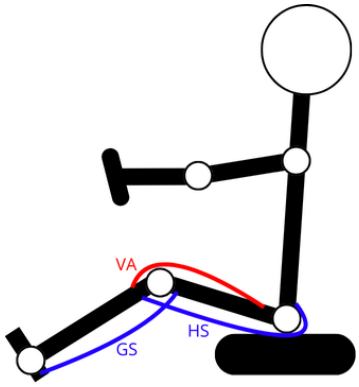

(b) Lombard's Paradox visualized, with the monoarticular Vasti (VA) and biarticular hamstring (HS) muscles and Gastrocnemii (GS). Contraction of VA with HS and GS acting as tendons would result in ankle plantarflexion, knee flexion, and hip extension.

Figure 4.1: Schematic of a rower mid-drive, showing monoarticular muscles in red and biarticular muscles in blue.

Lombard's paradox also explains why work at the joint level is concentrated at the hip, despite the Vasti contributing most of the work at the muscle level. Due to their tendinous behavior, the biarticular hamstring muscles only stretch slightly. As a result, little work is lost at the hamstrings, while a great deal of work is transferred from the knees to the hips allowing the Vasti to actuate two joints, minimizing total muscle activations. Other differences between the muscle level and the joint actuator level can also be attributed to this effect, albeit as a result of other biarticular muscles. Figure 4.1b also shows how the Gastrocnemii allows the Vasti to induce plantarflexion at the ankle.

4.2. Efficiency

From the results shown in section 3.3, as well as previous research by Hofmijster et al [23], which is supported by the results in Figure 3.2, no significant effect of power output or stroke rate on relative muscle contributions or metabolic efficiency can be identified with any certainty. Although Table 3.2 shows significant effects of both stroke rate and power output on elbow flexion, this is likely due to weakness of the Brachioradialis muscle. Since no statistically significant effect has been found at the joint level as well, the p-values for elbow flexion in Table 3.2 are disregarded.

As efficiency seems to be unaffected by stroke rate, the question remains why rowers show a preference for a specific stroke rate at a given power output. In theory, some metabolically optimal stroke rate should exist. Stroke rate cannot be increased or decreased without encountering the limitations of the human body. At an extremely low stroke rate of 1 stroke per minute, forces to maintain a reasonable power output cannot be attained, whereas at extremely high stroke rates of nearly 100 strokes per minute, the inertia of the human body will prevent the rower from changing direction fast enough to perform strokes. Two, and possibly more, explanations can be given as to why no optimum has currently been found. First, the preference for stroke rate at a given power output could be taught, since rowers often train in groups, where synchronizing the motion could be prioritized over rowing efficiently at the individual level. This could lead to rowers preferring a stroke rate that is not metabolically most efficient, explaining the absence of a peak in metabolic efficiency at preferred stroke rate. Second, the optimum might not be as clear as in other endurance sports. The optimum might exhibit a relatively flat range of frequencies at which efficiency is at its highest, instead of a clear peak at one frequency. This could be caused by the factors above (i.e. inertia and muscle strength) having different optima, which cancel each other out across the tested range. Additionally, rowing strokes consist of two very distinct phases. It is conceivable that the recovery phase in fact enables a rower to recover from the drive phase, enabling the rower to perform some anaerobic work, in addition to aerobic work.

4.3. Implications

The results in this report give a deeper insight into muscle dynamics in ergometer rowing, which paves the way for more detailed studies of rowing technique. Although the results of this study will not directly

affect rowing performance, insights into relative muscle contributions and how work is distributed across joints by muscles could be used by coaches to improve training programs to train muscles in ways that correspond to actual rowing. When applying the findings of this research to alter training programs, the role of biarticular muscles such as the hamstrings should be considered, as it is the combined effort of the quadriceps and the hamstrings that brings about knee and hip extension during the drive.

Translating these insights from an ergometer to on-water rowing is possible to a certain extent, but should only be done when taking into account the differences between on-water rowing and ergometer rowing [27], [31]. The use of an ergometer for this research simplified data acquisition by eliminating environmental conditions such as wind and temperature, allowing for the collection of a more comprehensive dataset. However, it simplifies the rowing motion, as the motion performed on an ergometer is more linear and symmetric.

The model used to generate muscle results in this research can be expanded to on-water rowing. This would allow for more in-depth analyses of the differences between on-water and ergometer rowing in terms at the muscle level. Additionally, the model could then be used to further analyze differences between scull and oar rowing [24].

4.4. Validity and limitations

Several checks have been performed to validate model results for steady state ergometer rowing after each simulation step. With the marker errors, residuals, reserves, and correlations and MAE found in section 3.2, we deem model results to be accurate for all muscles, except for the Brachioradialis, which is too weak to fully sustain the elbow flexion moment needed in the rowing motion. The lower body validation results are particularly good, with lower marker errors and reserves than around the shoulder. Nevertheless, comparison of SO results to EMG measurements shows good agreement between measured and simulated muscle dynamics for both leg and shoulder muscles.

The model has been validated for steady state ergometer rowing specifically. Significant differences exist between the start of rowing [44] and steady state rowing, as more power is generally generated during the start. During the starting phase, as well as in sprinting, muscle forces are more often limited to the condition of ensuring continuous contact with the seat. Therefore, additional analysis should be done on the starts of the trials, as well as the sprints at the end of the 75% PO trials measured in the experiment to assess muscle dynamics in these conditions.

Additionally, differences between ergometer rowing and on-water should be taken into account when interpreting the results presented in this report for improving on-water rowing training programs. Although muscle recruitment is similar [26], [31], [43], ergometer training should not be viewed as a substitute for on-water rowing, but rather as cross training [27]. In order to gain insights into muscle contributions during on-water rowing, the model used in this report should be used with on-water experimental data in order to validate the model and generate results.

It should be noted that the current experiment only recruited male participants. This was done in order to ensure better agreement between collected data and the musculoskeletal model, which is also based on male subjects. However, this choice does maintain the bias present in musculoskeletal analysis [35]. Collecting experimental data of female rowers and building a female version of the model should be regarded as an important next step, in order to reduce the gap in female representation in biomechanical analysis [28].

Another potential improvement of the model would be to incorporate abdominal and back muscles. From the reserve actuators in Figures 3.8-3.10, it is apparent that these muscles do add work to the system. Additionally, some bending could be added to the rigid spine in the current model. This would improve the validity of the motion at the neck and shoulders, and likely also have an effect on abdominal and back muscles.

In this report, only 5 out of 14 participants have been analyzed. This likely has an effect on the significance levels in Table 3.2. Inclusion of the other 9 participants could help pinpoint a direction for further research in order to explain preferences of rowers for a specific stroke rate.

To attain better agreement between SO results and EMG, correlation and MAE can be improved by

accounting for electromechanical delay and improving the normalization protocol respectively. Incorporating electromechanical delay will shift SO and EMG output signals to match better over the entire stroke. As for the normalization protocol, the current method is appropriate for most muscles, except for Gluteus Maximus and Anterior Deltoid. Performing separate maximum voluntary contraction trials for these muscles could improve normalization in these muscles.

5

Conclusion

This report describes the analysis of muscle contributions to total work in ergometer rowing. This analysis yields the following key findings:

- The quadriceps, and mainly Vastus Lateralis, are the largest contributors of work in ergometer rowing. Other strong contributors include Soleus at the calves, Gluteus Maximus at the hip, and Brachioradialis at the elbow. Erector Spinae is not included in the model, but its EMG measurements and the contribution of the lumbar actuators suggest that it plays an important role in generating power in the lower back.
- Biarticular muscles play an important role in distributing work over joints in ergometer rowing. As explained by Lombard's paradox, hamstrings do little work, but act as tendons to enable the Vasti to extend both the knee and hip joints.
- No significant effect of either stroke rate or power output could be found on muscle coordination. Additionally, no significant effect has been found on metabolic efficiency, despite indications that some metabolically optimal stroke rate should exist. Some hypotheses are presented to explain the absence of this optimum in current data. Most likely, some optimum exists, but exhibits a relatively flat peak, caused by underlying factors having different optima.

Additionally, this report shows the process of gathering a comprehensive dataset on ergometer rowing, validation of a combined musculoskeletal model containing leg and shoulder muscles, and analysis of simulation results obtained from this musculoskeletal model using data from the experiment. The data collected in the experiment can be used for further analysis on effects of power output and stroke rate on various aspects of rowing technique. The musculoskeletal model can be used to gain more detailed insights on rowing technique, specifically at the muscle level, although it should be noted that Brachioradialis might need rescaling to more accurately represent trained athletes.

Recommendations and future work

The model used in this research is currently limited to analysis on ergometer rowing for male subjects. Logical next steps in this research would thus be to either build a similar model suitable for female subjects or to validate the model for on-water rowing, in which movements are less symmetrical and linear. Additionally, it could be interesting to add muscles and DOFs at the wrist and back, allowing plantarflexion and ulnar deviation at the wrist and bending of the spine in the model. This could give further insights into muscle contributions in all relevant joints.

With the analyses of leg and shoulder muscles in this report, it would be interesting to investigate whether relative muscle contributions might change outside of the ranges measured in the experiment. In particular, muscle coordination at the start of each trial, as well as the data from the sprint at the end of the 75% 2K PO trial could be analyzed, as the objective to generate maximal power output differs from maintaining a certain power output over prolonged periods of time in a steady state.

References

[1] M. M. Alemi, J. J. Banks, A. C. Lynch, B. T. Allaire, M. L. Bouxsein, and D. E. Anderson, "EMG Validation of a Subject-Specific Thoracolumbar Spine Musculoskeletal Model During Dynamic Activities in Older Adults," en, *Annals of Biomedical Engineering*, vol. 51, no. 10, pp. 2313–2322, Oct. 2023.

[2] M. S. Andersen, "4 - Introduction to musculoskeletal modelling," in *Computational Modelling of Biomechanics and Biotribology in the Musculoskeletal System (Second Edition)*, ser. Woodhead Publishing Series in Biomaterials, Z. Jin, J. Li, and Z. Chen, Eds., Woodhead Publishing, Jan. 2021, pp. 41–80.

[3] L. Ansley and P. Cangley, "Determinants of "optimal" cadence during cycling," *European Journal of Sport Science*, vol. 9, no. 2, pp. 61–85, Mar. 2009.

[4] M. Boland, N. M. Crotty, N. Mahony, B. Donne, and N. Fleming, "A Comparison of Physiological Response to Incremental Testing on Stationary and Dynamic Rowing Ergometers," en, *International Journal of Sports Physiology and Performance*, vol. 17, no. 4, pp. 515–522, Apr. 2022.

[5] J. Brisswalter, C. Hausswirth, D. Smith, F. Vercruyssen, and J. M. Vallier, "Energetically Optimal Cadence vs. Freely-Chosen Cadence During Cycling: Effect of Exercise Duration," en, *International Journal of Sports Medicine*, vol. 21, pp. 60–64, Dec. 2000.

[6] T. Cerne, R. Kamnik, B. Vesnicer, J. Zganec Gros, and M. Munih, "Differences between elite, junior and non-rowers in kinematic and kinetic parameters during ergometer rowing," eng, *Human Movement Science*, vol. 32, no. 4, pp. 691–707, Aug. 2013.

[7] V. D. Chandran, R. L. Lambach, R. S. Gibbons, B. J. Andrews, G. S. Beaupre, and S. Pal, "Tibiofemoral forces during FES rowing in individuals with spinal cord injury," *Computer Methods in Biomechanics and Biomedical Engineering*, vol. 24, no. 3, pp. 231–244, Feb. 2021.

[8] L. Chiari, U. D. Croce, A. Leardini, and A. Cappozzo, "Human movement analysis using stereophotogrammetry: Part 2: Instrumental errors," *Gait & Posture*, vol. 21, no. 2, pp. 197–211, Feb. 2005.

[9] C. E. Clauser, J. T. Mcconville, and J. W. Young, "WEIGHT, VOLUME, AND CENTER OF MASS OF SEGMENTS OF THE HUMAN BODY," en, Aug. 1969.

[10] C. J. Clemente, F. De Groote, and T. J. M. Dick, "Predictive musculoskeletal simulations reveal the mechanistic link between speed, posture and energetics among extant mammals," en, *Nature Communications*, vol. 15, no. 1, p. 8594, Oct. 2024.

[11] D. M. Corcos, G. L. Gottlieb, M. L. Latash, G. L. Almeida, and G. C. Agarwal, "Electromechanical delay: An experimental artifact," en, *Journal of Electromyography and Kinesiology*, vol. 2, no. 2, pp. 59–68, Jan. 1992.

[12] M. P. DE LOOZE, I. KINGMA, W. THUNNISSEN, M. J. VAN WIJK, and H. M. TOUSSAINT, "The evaluation of a practical biomechanical model estimating lumbar moments in occupational activities," *Ergonomics*, vol. 37, no. 9, pp. 1495–1502, Sep. 1994.

[13] C. J. De Luca, L. Donald Gilmore, M. Kuznetsov, and S. H. Roy, "Filtering the surface EMG signal: Movement artifact and baseline noise contamination," *Journal of Biomechanics*, vol. 43, no. 8, pp. 1573–1579, May 2010.

[14] U. Della Croce, A. Leardini, L. Chiari, and A. Cappozzo, "Human movement analysis using stereophotogrammetry: Part 4: Assessment of anatomical landmark misplacement and its effects on joint kinematics," *Gait & Posture*, vol. 21, no. 2, pp. 226–237, Feb. 2005.

[15] S. L. Delp, F. C. Anderson, A. S. Arnold, *et al.*, "OpenSim: Open-Source Software to Create and Analyze Dynamic Simulations of Movement," en, *IEEE Transactions on Biomedical Engineering*, vol. 54, no. 11, pp. 1940–1950, Nov. 2007.

[16] Y. Duchene, F. R. Simon, G. N. Ertel, H. Maciejewski, G. C. Gauchard, and G. Mornieux, “The stroke rate influences performance, technique and core stability during rowing ergometer,” *Sports Biomechanics*, vol. 0, no. 0, pp. 1–18, Jan. 2024.

[17] B. Elliott, A. Lyttle, and O. Birkett, “Rowing: The RowPerfect Ergometer: A training aid for on□water single scull rowing,” en, *Sports Biomechanics*, vol. 1, no. 2, pp. 123–134, Jul. 2002.

[18] N. Fleming, B. Donne, and N. Mahony, “A comparison of electromyography and stroke kinematics during ergometer and on-water rowing,” *Journal of Sports Sciences*, vol. 32, no. 12, pp. 1127–1138, Jul. 2014.

[19] K. Hase, S. E. Halliday, and A. B. Zavatsky, “A COMPREHENSIVE BIOMECHANICAL STUDY OF ERGOMETER ROWING WITH MUSCULOSKELETAL MODELS,” en, 2003.

[20] J. L. Hicks, T. K. Uchida, A. Seth, A. Rajagopal, and S. L. Delp, “Is My Model Good Enough? Best Practices for Verification and Validation of Musculoskeletal Models and Simulations of Movement,” *Journal of Biomechanical Engineering*, vol. 137, no. 020905, Feb. 2015.

[21] H. Hill, “Dynamics of coordination within elite rowing crews: Evidence from force pattern analysis,” *Journal of Sports Sciences*, vol. 20, no. 2, pp. 101–117, Jan. 2002.

[22] M. J. Hofmijster, A. J. Van Soest, and J. J. De Koning, “Rowing Skill Affects Power Loss on a Modified Rowing Ergometer,” en-US, *Medicine & Science in Sports & Exercise*, vol. 40, no. 6, p. 1101, Jun. 2008.

[23] M. J. Hofmijster, A. J. Van Soest, and J. J. De Koning, “Gross Efficiency during Rowing Is Not Affected by Stroke Rate,” en, *Medicine & Science in Sports & Exercise*, vol. 41, no. 5, pp. 1088–1095, May 2009.

[24] P. A. Hume, “Movement analysis of scull and oar rowing,” English, in *Handbook of Human Motion*, B. Müller and S. I. Wolf, Eds., vol. 2-3, Springer International Publishing, 2018, pp. 1719–1739.

[25] I. Hunter and G. A. Smith, “Preferred and optimal stride frequency, stiffness and economy: Changes with fatigue during a 1-h high-intensity run,” en, *European Journal of Applied Physiology*, vol. 100, no. 6, pp. 653–661, Aug. 2007.

[26] V. Kleshnev, “THE EFFECTS OF STROKE RATE ON BIOMECHANICAL PARAMETERS AND EFFICIENCY OF ROWING,” en, 1996.

[27] V. Kleshnev, *The biomechanics of rowing: a unique insight into the technical and tactical aspects of elite rowing*, eng, Revised 2. edition. Marlborough: Crowood, 2022.

[28] E. van der Kruk, “BIASMECHANICS: Does an unconscious bias still persist in biomechanics, positioning males as the default in human research? A meta-analysis on the Journal of Biomechanics 2024 publications,” *Journal of Biomechanics*, vol. 181, p. 112 560, Mar. 2025.

[29] E. van der Kruk and M. M. Reijne, “Accuracy of human motion capture systems for sport applications; state-of-the-art review,” *European Journal of Sport Science*, vol. 18, no. 6, pp. 806–819, Jul. 2018.

[30] A. D. Kuo, “THE ACTION OF TWO-JOINT MUSCLES: THE LEGACY OF W. P. LOMBARD,” en, *Classics in Movement Science*, vol. 10, pp. 289–315, 2002.

[31] D. H. Lamb, “A kinematic comparison of ergometer and on-water rowing,” eng, *The American Journal of Sports Medicine*, vol. 17, no. 3, pp. 367–373, 1989.

[32] A. Leardini, L. Chiari, U. D. Croce, and A. Cappozzo, “Human movement analysis using stereophotogrammetry: Part 3. Soft tissue artifact assessment and compensation,” *Gait & Posture*, vol. 21, no. 2, pp. 212–225, Feb. 2005.

[33] W. P. Lombard, “The Action of Two-Joint Muscles,” EN, *American Physical Education Review*, Sep. 1903.

[34] M. E. Lund, M. de Zee, M. S. Andersen, and J. Rasmussen, *On validation of multibody musculoskeletal models*, en, 2012.

[35] R. Maarleveld, H. E. J. Veeger, F. C. T. v. d. Helm, J. Son, R. L. Lieber, and E. v. d. Kruk, *What the %PCSA? Addressing Diversity in Lower-Limb Musculoskeletal Models: Age- and Sex-related Differences in PCSA and Muscle Mass*, Nov. 2024.

[36] K. Matsui, K. Shimada, and P. D. Andrew, “Deviation of skin marker from bone target during movement of the scapula,” *Journal of Orthopaedic Science*, vol. 11, no. 2, pp. 180–184, Mar. 2006.

[37] B. T. v. Oeveren, C. J. d. Ruiter, P. J. Beek, and J. H. v. Dieën, “Optimal stride frequencies in running at different speeds,” en, *PLOS ONE*, vol. 12, no. 10, e0184273, Oct. 2017.

[38] “Over de KNRB.” nl-NL. (), [Online]. Available: `https://knrb.nl/over-knrb/` (visited on 07/22/2025).

[39] M. Retailleau, P. Fisette, and F. Colloud, “A closed-loop multibody model to assess lower-limb kinematics in rowing,” *Computer Methods in Biomechanics and Biomedical Engineering*, vol. 22, no. sup1, S345–S347, May 2019.

[40] C. J. de Ruiter, S. van Daal, and J. H. van Dieën, “Individual optimal step frequency during outdoor running,” *European Journal of Sport Science*, vol. 20, no. 2, pp. 182–190, Feb. 2020.

[41] A. Seth, M. Dong, R. Matias, and S. Delp, “Muscle Contributions to Upper-Extremity Movement and Work From a Musculoskeletal Model of the Human Shoulder,” eng, *Frontiers in Neurorobotics*, vol. 13, p. 90, 2019.

[42] A. Seth, J. L. Hicks, T. K. Uchida, *et al.*, “OpenSim: Simulating musculoskeletal dynamics and neuromuscular control to study human and animal movement,” en, *PLOS Computational Biology*, vol. 14, no. 7, D. Schneidman, Ed., e1006223, Jul. 2018.

[43] T. B. Smith and W. G. Hopkins, “Measures of Rowing Performance,” en, *Sports Medicine*, vol. 42, no. 4, pp. 343–358, Apr. 2012.

[44] A. “. van Soest and M. Hofmijster, “Strapping rowers to their sliding seat improves performance during the start of ergometer rowing,” *Journal of Sports Sciences*, vol. 27, no. 3, pp. 283–289, Feb. 2009.

[45] X. Suo, W. Tang, and Z. Li, “Motion Capture Technology in Sports Scenarios: A Survey,” en, *Sensors*, vol. 24, no. 9, p. 2947, Jan. 2024.

[46] G. Treff, L. Mentz, B. Mayer, K. Winkert, T. Engleder, and J. M. Steinacker, “Initial Evaluation of the Concept-2 Rowing Ergometer’s Accuracy Using a Motorized Test Rig,” English, *Frontiers in Sports and Active Living*, vol. 3, Jan. 2022.

[47] J. Troy Blackburn, D. R. Bell, M. F. Norcross, J. D. Hudson, and L. A. Engstrom, “Comparison of hamstring neuromechanical properties between healthy males and females and the influence of musculotendinous stiffness,” *Journal of Electromyography and Kinesiology*, vol. 19, no. 5, e362–e369, Oct. 2009.

[48] N. A. Turpin, A. Guével, S. Durand, and F. Hug, “Effect of power output on muscle coordination during rowing,” en, *European Journal of Applied Physiology*, vol. 111, no. 12, pp. 3017–3029, Dec. 2011.

[49] S. D. Uhlrich, R. W. Jackson, A. Seth, J. A. Kolesar, and S. L. Delp, “Muscle coordination retraining inspired by musculoskeletal simulations reduces knee contact force,” eng, *Scientific Reports*, vol. 12, no. 1, p. 9842, Jul. 2022.

[50] J.-M. J. Wilson, D. G. E. Robertson, and J. P. Stothart, “Analysis of Lower Limb Muscle Function in Ergometer Rowing,” en, *International Journal of Sport Biomechanics*, vol. 4, no. 4, pp. 315–325, Nov. 1988.

[51] M. Żuk, M. Syczewska, and C. Pezowicz, “Use of the surface electromyography for a quantitative trend validation of estimated muscle forces,” *Biocybernetics and Biomedical Engineering*, vol. 38, no. 2, pp. 243–250, Jan. 2018.

A

Overview of markers and muscles measured during the experiment

This appendix presents an overview of markers and muscles measured in the experiment. Figure A.1 shows the setup with all measurement systems visible, Figure A.2 shows all muscles measured through EMG, and Tables A.1 and A.2 list the markers measured during the experiment.

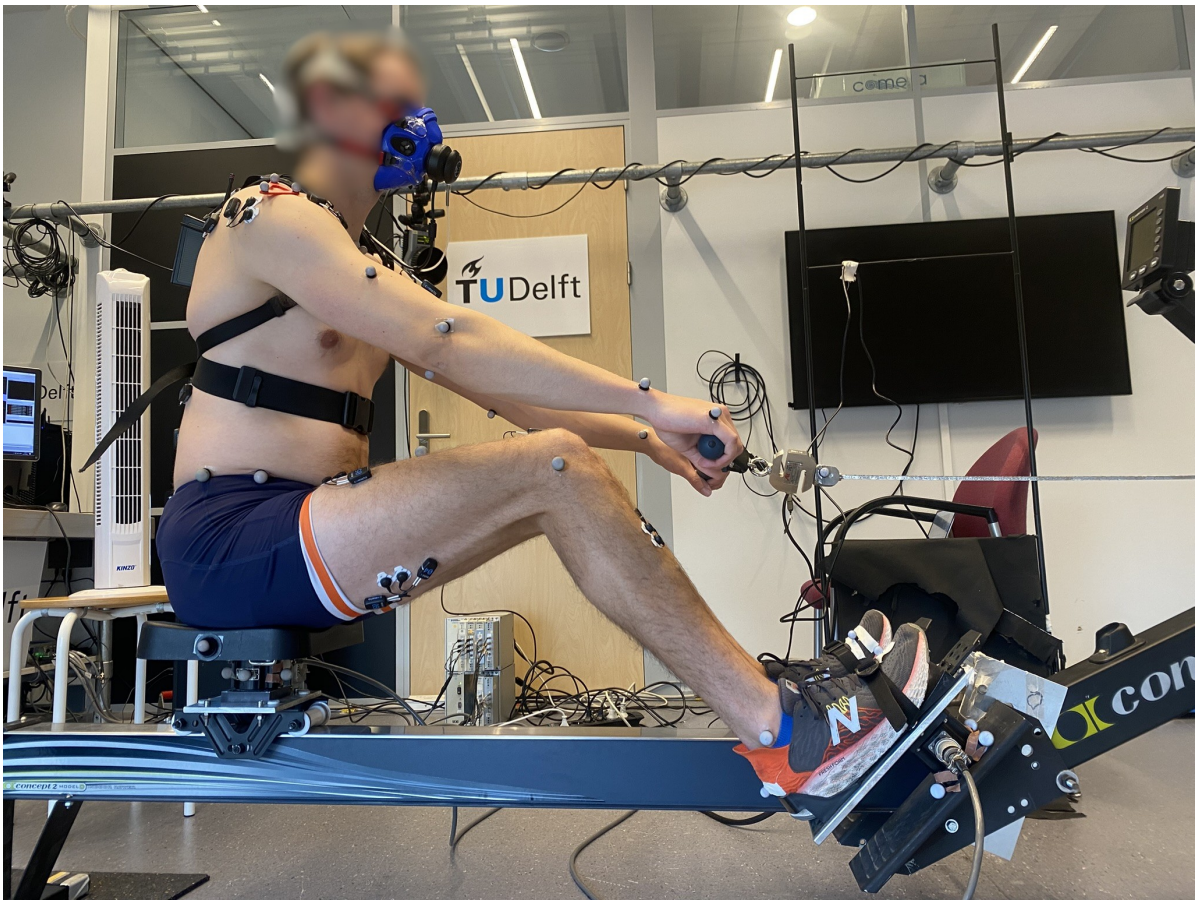

Figure A.1: Experimental setup showing the measurement systems.

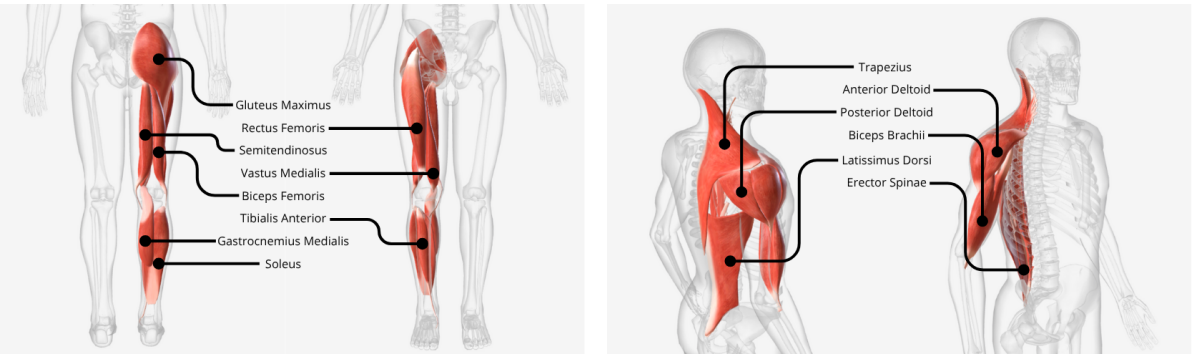

(a) Leg muscles

(b) Shoulder muscles

Figure A.2: Posterior (left) and anterior (right) view of all muscles measured in the experiment through EMG.

Table A.1: Marker locations for all body markers used in the experiment.

Body markers	Location
LToes	Left toes
LMal_Med	Left medial malleolus
LMal_Lat	Left lateral malleolus
LHeel	Left heel
LShank	Left shank
LKnee_Lat	Left lateral malleolus
LKnee_Med	Left medial malleolus
LThigh	Left thigh
LASIS	Left ASIS
LPelvisSide	Left pelvis side
LPSIS	Left PSIS
RToes	Left toes
RMal_Med	Right medial malleolus
RMal_Lat	Right lateral malleolus
RHeel	Right heel
RShank	Right shank
RKnee_Lat	Right lateral knee
RKnee_Med	Right medial knee
RThigh	Right thigh
RASIS	Right ASIS
RPelvisSide	Right pelvis side
RPSIS	Right PSIS
C7	C7 vertebra
LCS	Left clavicle - sternum
LClav	Left clavicle - acromion
LHum	Left humerus
LElbow_Med	Left medial elbow
LElbow_Lat	Left lateral elbow
LWristR	Left wrist radius
LWristU	Left wrist ulna
LIndex	Left index metacarpalphalangeal joint
LPinkie	Left pinkie metacarpalphalangeal joint
RCS	Right clavicle - sternum
RClav	Right clavicle - acromion
RHum	Right humerus
RElbow_Med	Right medial elbow
RElbow_Lat	Right lateral elbow
RWristR	Right wrist radius
RWristU	Right wrist ulna
RIndex	Right index metacarpalphalangeal joint
RPinkie	Right pinkie metacarpalphalangeal joint
ScapTriadL	Scapula triad - left from Lclav
ScapTriadP	Scapula triad - posterior from Lclav
ScapUL	Scapula upper left
ScapUR	Scapula upper right
ScapB	Scapula bottom

Table A.2: Marker locations for all markers on the setup used in the experiment.

Setup markers	Location
SeatL	Left side of seat
SeatR	Right side of seat
SeatB	Back of the seat
Seat_B	Back of seat force sensor
Seat_F	Front of seat force sensor
LFoot_LL	Left foot stretcher sensor - lower left
LFoot_UL	Left foot stretcher sensor - upper left
LFoot_UR	Left foot stretcher sensor - upper right
RFoot_LR	Right foot stretcher sensor - lower right
RFoot_UR	Right foot stretcher sensor - upper right
RFoot_UL	Right foot stretcher sensor - upper left
HandleL	Handle force sensor - left side
HandleR	Handle force sensor - right side
ChainL	Ergometer - left of chain hole
Broom1	Broomstick - proximal marker
Broom2	Broomstick - distal marker

B

Overview of muscles and DOFs included in the model

In this appendix, an overview of the OpenSim model is outlined. Figure B.1 shows the muscles in the model in anatomical position. Figure B.2 does the same for the model markers. Figure B.3 shows the model markers and muscles with the model in a rowing position. Finally, Tables B.1 and B.2 list all muscles and degrees of freedom in the model.

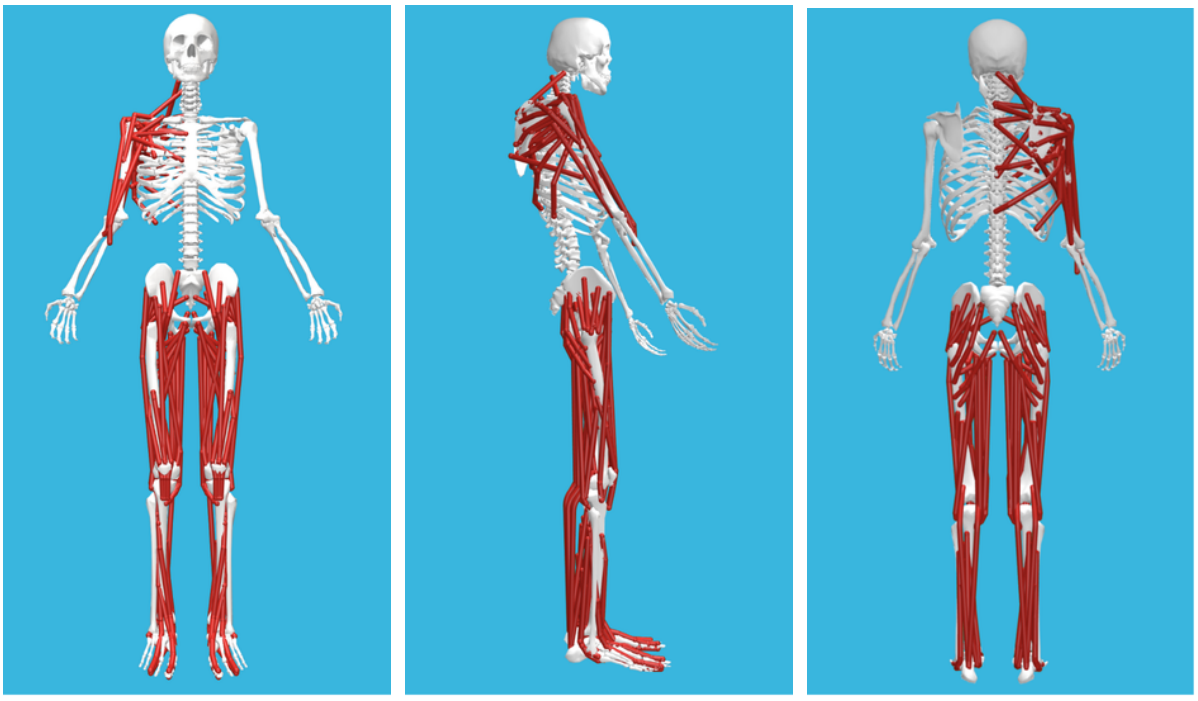

(a) Anterior view. **(b)** Sagittal view. **(c)** Posterior view.

Figure B.1: Model muscles in OpenSim.

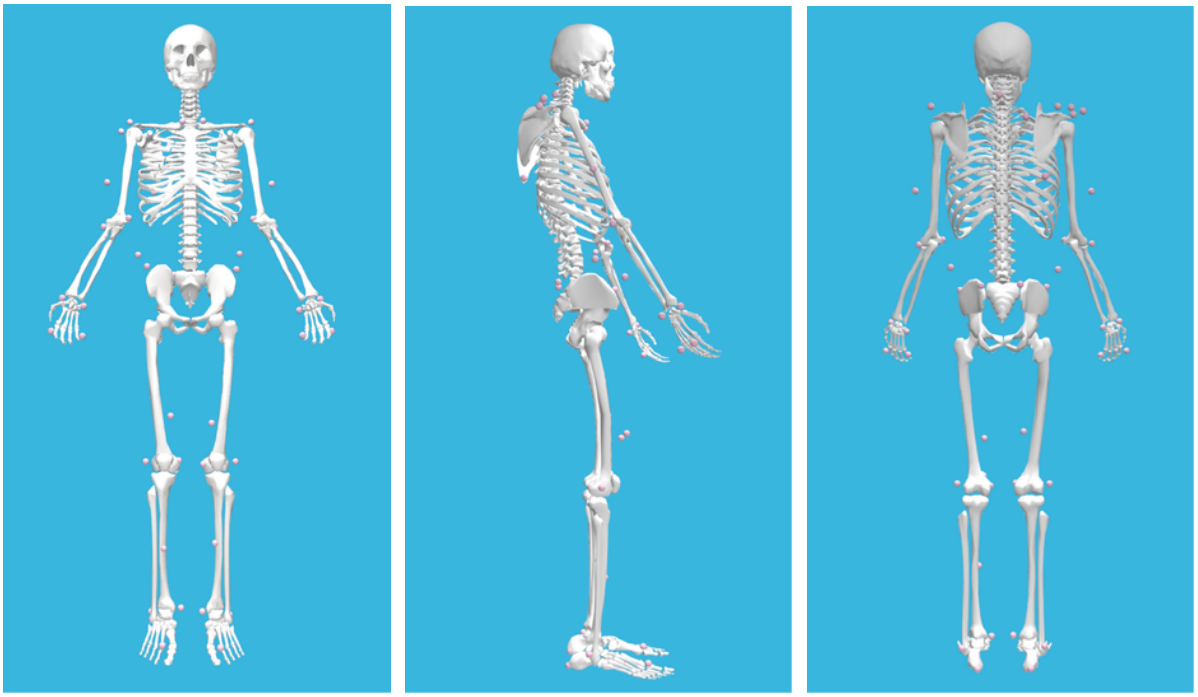

(a) Anterior view. **(b)** Sagittal view. **(c)** Posterior view.

Figure B.2: Model marker locations in OpenSim.

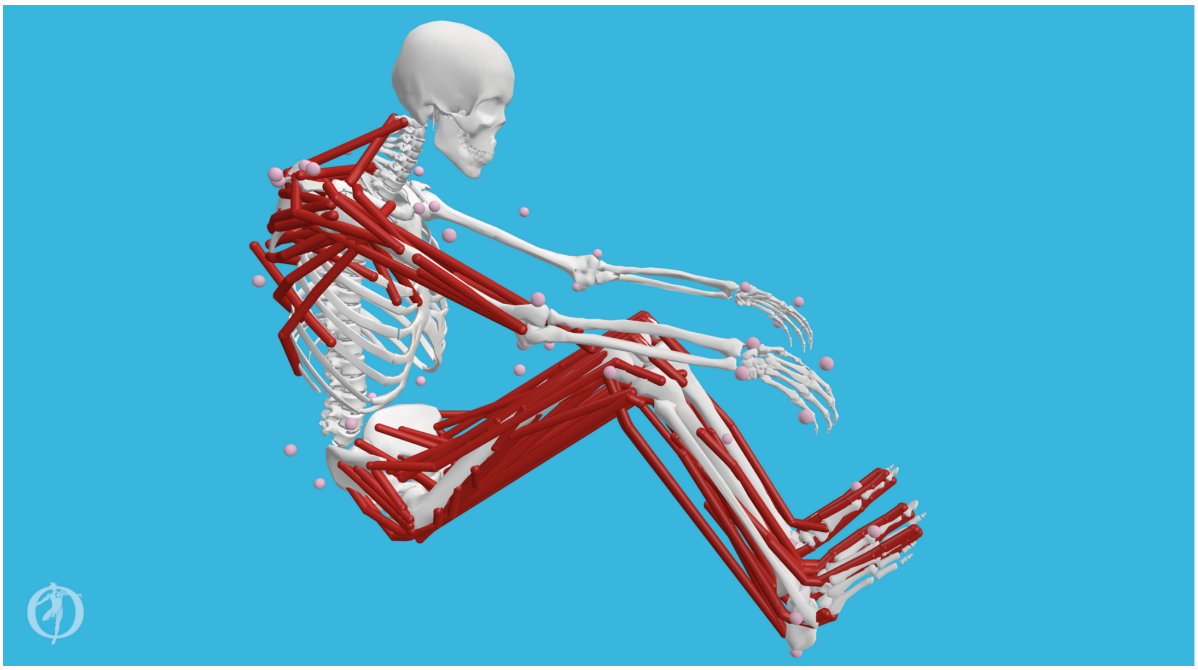

Figure B.3: OpenSim model showing model geometry, all markers, and muscle segments in a rowing position.

Table B.1: Muscle (segments) present in the model and their full names. muscles with an asterisk (*) are also present on the left side, with _l as suffix instead of _r.

Model muscles	Name	Segment
BRA	Brachioradialis	
TrapeziusScapula_M	Trapezius	Scapula, Medius
TrapeziusScapula_S	Trapezius	Scapula, Superior
TrapeziusScapula_I	Trapezius	Scapula, Inferior
TrapeziusClavicle_S	Trapezius	Clavicle
SerratusAnterior_I	Serratus Anterior	Inferior
SerratusAnterior_M	Serratus Anterior	Medius
SerratusAnterior_S	Serratus Anterior	Superior
Rhomboideus_S	Rhomboideus	Superior
Rhomboideus_I	Rhomboideus	Inferior
LevatorScapulae	Levator Scapulae	
Coracobrachialis	Coracobrachialis	
DeltoideusClavicle_A	Deloid	Anterior
DeltoideusScapula_P	Deltoid	Posterior
DeltoideusScapula_M	Deltoid	Medius
LatissimusDorsi_S	Latissimus Dorsi	Superior
LatissimusDorsi_M	Latissimus Dorsi	Medius
LatissimusDorsi_I	Latissimus Dorsi	Inferior
PectoralisMajorClavicle_S	Pectoralis Major	Clavicle, Superior
PectoralisMajorThorax_I	Pectoralis Major	Thorax, Inferior
PectoralisMajorThorax_M	Pectoralis Major	Thorax, Medius
TeresMajor	Teres Major	
Infraspinatus_I	Infraspinatus	Inferior
Infraspinatus_S	Infraspinatus	Superior
PectoralisMinor	Pectoralis Minor	
TeresMinor	Teres Minor	
Subscapularis_S	Subscapularis	Superior
Subscapularis_M	Subscapularis	Medius
Subscapularis_I	Subscapularis	Inferior
Supraspinatus_P	Supraspinatus	Posterior
Supraspinatus_A	Supraspinatus	Anterior
TRI_long	Triceps Brachii	Long head
TRI_med	Triceps Brachii	Medial
TRI_lat	Triceps Brachii	Lateral
BIC_long	Biceps Brachii	Long head
BIC_brevis	Biceps Brachii	Short head
addbrev_r*	Adductor Brevis	
addlong_r*	Adductor Longus	
addmagDist_r*	Adductor Magnus	Distal
addmagIsch_r*	Adductor Magnus	Ischial
addmagMid_r*	Adductor Magnus	Middle
addmagProx_r*	Adductor Magnus	Proximal
bflh_r*	Biceps Femoris	Long head
bfsh_r*	Biceps Femoris	Short head
edl_r*	Extensor Digitorum Longus	
ehl_r*	Extensor Hallucis Longus	
fdl_r*	Flexor Digitorum Longus	
fhl_r*	Flexor Hallucis Longus	
gaslat_r*	Gastrocnemius Lateralis	
gasmed_r*	Gastrocnemius Medialis	
glmax1_r*	Gluteus Maximus	
glmax2_r*	Gluteus Maximus	
glmax3_r*	Gluteus Maximus	
glmed1_r*	Gluteus Medius	
glmed2_r*	Gluteus Medius	
glmed3_r*	Gluteus Medius	
glmin1_r*	Gluteus Minimus	
glmin2_r*	Gluteus Minimus	
glmin3_r*	Gluteus Minimus	
grac_r*	Gracilis	
iliacus_r*	Iliacus	
perbrev_r*	Peroneus Brevis	
perlong_r*	Peroneus Longus	
piri_r*	Piriformis	
psoas_r*	Psoas	
recfem_r*	Rectus Femoris	
sart_r*	Sartorius	
semimem_r*	Semimembranosus	
semiten_r*	Semitendinosus	
soleus_r*	Soleus	
tfl_r*	Tensor Fasciae Latae	
tibant_r*	Tibialis Anterior	
tibpost_r*	Tibialis Posterior	
vasint_r*	Vastus Intermedius	
vaslat_r*	Vastus Lateralis	
vasmed_r*	Vastus Medialis	

Table B.2: Degrees of freedom in the model and their full names. DOFs with an asterisk (*) are also present on the left side, with _l as suffix instead of _r

Model DOF	Full name
pelvis_tx	Pelvis translation x
pelvis_ty	Pelvis translation y
pelvis_tz	Pelvis translation z
pelvis_tilt	Pelvis tilt
pelvis_list	Pelvis list
pelvis_rot	Pelvis rotation
hip_flex_r*	Hip flexion
hip_add_r*	Hip adduction
hip_rot_r*	Hip rotation
knee_angle_r*	Knee flexion
ankle_angle_r*	Ankle plantarflexion
subtalar_angle_r*	Ankle inversion
mtp_angle_r*	Metatarsophalangeal flexion
lumbar_ext	Lumbar extension
lumbar_bend	Lumbar bending
lumbar_rot	Lumbar rotation
clav_prot_r*	Clavicle protrusion
clav_elev_r*	Clavicle elevation
scapula_abduction_r*	Scapula abduction
scapula_winging_r*	Scapula winging
scapula_elevation_r*	Scapula elevation
scapula_upward_rot_r*	Scapula upward rotation
plane_elv_r*	Plane elevation
shoulder_elev_r*	Shoulder elevation
axial_rot_r*	Axial rotation
elbow_flex_r*	Elbow flexion
pro_sup_r*	Pronation/supination